Engineering Geology 316 (2023) 107046

Contents lists available at ScienceDirect

Engineering Geology

journal homepage: www.elsevier.com/locate/enggeo

SHAKER: A selector of consistent and energetically equalized natural ground motions using the Italian earthquake database

Gerardo Grelle [a,*], Giuseppe Sappa [a], Claudia Madiai [b]

[a] Department of Civil, Constructional and Environmental Engineering – DICEA, Sapienza University of Rome, Italy
[b] Department of Civil and Environmental Engineering – DICEA, University of Study of Florence, Italy

ARTICLE INFO

Keywords:
Seismic hazard
Ground motions selector tool
Housner Intensity
Ground motion parametrization
Consistency analysis

ABSTRACT

Input motion set selection for nonlinear dynamic structural analysis is commonly based on spectral compatibility, obtained through the uniform scaling of natural signals. Due to the aleatory nature of the expected time history, alone spectral compatibility requirement appears very weak to guarantee scaled ground motions that suit local seismic hazard. Magnitude-Distance interval pairs to control selection and scaling factor thresholds do not always provide input motions with adequate energy levels. In order to tackle these critical issues, a novel computer-aided selection method based on consistency analysis to provide conservative energy levels has been developed. The method equalizes the ground motions subject to the spectral compatibility process to the modified Housner Intensity of the hazard spectra. A multi-parametric consistency analysis based on statistic confidence is performed on the equalized (by uniform scaling) ground motion set by comparing it with the larger regional natural dataset on the same Magnitude-Distance pairs. The consistency analysis involves multiple ground motion parameters taken into relation with the focal mechanism too. Sensitivity tests show the capability of the method to reach high spectral compatibility joined with high consistency degrees by multi-parametric calibration. Compared with the traditional ones, this method also shows greater performance in composing ground motion sets close to real occurrences with a more assorted spectral frequency distribution.

1. Introduction

A well-founded selection of input ground motions is essential when performing seismic design and assessment of structural and geotechnical systems through non-linear dynamic analyses. This has been the object of several studies (among them: Alatik and Abrahamson, 2010; Baker and Lee, 2018; Beyer and Bommer, 2007; Du et al., 2006; Gao et al., 2014; Hancock et al., 2006; Iervolino et al., 2010; Iervolino and Cornell, 2005; Kottke and Rathje, 2008; Lanzo et al., 2015; Manfredi et al., 2022; Iervolino et al., 2018; Lombardi and de Luca, 2018). In this framework, some International Building Codes (Italian technical codes NTC-2018, EC8, FEMA P-1050/2015, ATC-40) (Cattari et al., 2018; International Code Council (ICC), 2018) provide median damped spectra, reflecting the base seismic hazard and accounting for stratigraphic and topographic features at the site. These uniform hazard response spectra can be used as the target for the response spectra of either natural (real), artificial, or simulated input ground motions. The match, with maximum and minimum tolerance, that is often referred to as "spectral compatibility" can be limited to an interval of periods of vibration of interest for the structure under study.

In accordance with recent building codes, the use of either artificial or simulated waveforms is allowed, yet with several requirements and limitations, but the use of uniform-scaled (or unscaled) natural ground motion sets is encouraged. In fact, natural ground motion sets ensure the conservation of the natural frequency distribution, also with respect to magnitude and distance (Bommer and Acevedo, 2004). Moreover, they are available in large databases such as the USGS Catalog, the PEER Strong Ground Motion Database, and the European Strong Motion (ESMD); the Italian ITACA database covers a significant portion of the latter. However, compatible ground motion sets from scaled natural records may present some criticalities, since they are composed with the only goal of finding the best match. As a consequence, possible inconsistencies between the hazard regional seismic features and the seismic energy interval of the selected waveforms may arise. When performing non-linear analyses with these ground motion sets, this issue may produce seismic energy under- or over-demands in civil engineering structures and geological natural systems (Decanini and Mollaioli, 2001; Ergun and Ates, 2014; Hildyard et al., 2009; Monti and Nisticò,

* Corresponding author.
E-mail address: gerardo.grelle@uniroma1.it (G. Grelle).

https://doi.org/10.1016/j.enggeo.2023.107046
Received 7 June 2022; Received in revised form 19 December 2022; Accepted 16 February 2023
Available online 24 February 2023
0013-7952/© 2023 Published by Elsevier B.V.

2002; Shiwua and Rutman, 2016; Wood and Hutchinson, 2012).

At a given site, seismic hazard is usually obtained using deterministic or probabilistic approaches (Rathje and Saygili, 2009; Angell et al., 2003; Cornell, 1969). They require the identification and characterization of all potential earthquake sources significantly affecting the seismicity of the site. Seismic hazard is expressed through several ground motion parameters, deriving from predictive relationships as a function of earthquake magnitude, M, and source-to-site distance (or epicentral distance), D (Ambraseys, 1995; Sabetta and Pugliese, 1996; Ambraseys et al., 1996). Disaggregation analysis is used to separate the contribution of M and D to the hazard (Galadini et al., 2012). Although this approach allows covering wide portions of seismically known areas, the values of parameters that completely characterize the ground motion, such as peak acceleration (PGA), spectral shape (as average-pseudo spectral acceleration, PSA, and predominant period), significant duration (Arias Intensity), and other ones, are generally difficult to define in a combined multiparametric manner. This difficulty stems from the regional and local variability of geotectonic features, such as fault depth, focal mechanisms, anisotropic and directional wave propagation, site effects, frequently combined with each other (Akkar et al., 2014; Bommer et al., 2000; Bommer and Crowley, 2006; Stafford and Bommer, 2009; Tsompanakis, 2014; Weatherill and Cotton, 2020; Woessner et al., 2015). Therefore, waveforms selected within a specific M-D interval can show inconsistencies if obtained from a multi-regional database that consists of signals with different geotectonic features. The scaling process generally introduces further inconsistencies in the spectral shape and energy content of the signals, when parametric restrictions are not included. Unusual energy levels and spectral shapes occur when scaling up far-source signals (with high D values). These signals conserve longer spectral periods due to combining wave dispersion effects and frequency-depending attenuation. In addition, far source signals are characterized by a longer duration produced by additional surface wave trains (Bommer et al., 2004; Goulet et al., 2007; Lasley et al., 2017; Thøgersen et al., 2019). Differently, a near-source signal tends to be an impulse signal with high PGA, containing short-period spectral energy (Xu et al., 2022). The use of unscaled ground motion sets can limit spectral atypicals, but the resulting sets suffer from the low assortment and frequently need to contain signals from large Magnitude-distance intervals to obtain spectral compatibility.

2. Background and motivations

Considering the natural effects influencing hazard by seismic shaking (in the time domain), selected input motion sets to end up having low correspondence with the physical laws controlling phenomena promoting it, when the ground motions composition of these sets is mainly oriented to fulfill spectral compatibility alone. On the other hand, uniform design spectra stem from shared regional hazard analysis and are reported so in national regulations, with direct implications on human activities in earthquake-prone areas. In these last few years, the structural and geological engineering community has become aware of the need for the combined consideration of these two critical issues and has proposed various processes, techniques, and methods to achieve it. Although these solutions take into account different influencing aspects separately or in combination, all are substantially communed by the same approach. This approach consists of controlling the selection by constraining signals to input seismological parameters in combined with thresholds to control scaling (Iervolino et al., 2010; Kottke and Rathje, 2008). As an integration, (Baker and Lee, 2018) proposed a statistical distribution of the target spectrum depending on the magnitude, distance and fault rupture mechanism, and a final optimization of ground motion set to fit that spectral distribution. Then, Corigliano et al. (2012) proposed a system founded on a database of rock recordings, in free-field conditions, extracted from various world databases (ESD, NGA, K-Net, and ITACA). This system is fundamentally based on spectral compatibility with scaling to even out PGA or another spectral ordinate; moreover, it favors spectral assortment by excluding the presence of components that belong to the same recording. Selections depending on soil category are provided by the system of Manfredi et al. (2022). A more complete version of this system typology was proposed by Sgobba et al. (2019). The system implements the past version of Iervolino et al. (2010) in the recent (online) version of the REXELweb code makes use of a supranational database: Engineering Strong-Motion database (ESM) (Luzi et al., 2016), related to the most tectonically active areas of the European continent. A preliminary selection finds signals according to the soil type (as EC8 classification) and the focal mechanism. In addition, mutually exclusive constraint criteria based on the values of Magnitude-distance and other seismic parameters are used. Unscaled and maximum scaling factor options control the ground motion set used in spectral compatibility. The system operates with reference to elastic spectra in pseudo-acceleration limited to 5% of the critical damping. Since the selection criteria are mutually exclusive, multiparametric coherence toward local hazard remains very difficult to check for selected waveforms. Considering the completeness of this last traditional system, it was used in the comparative analysis with the system object of this paper.

Here, an innovative computer selector system, based on a different approach compared to traditional systems, is proposed. This has been developed to minimize possible energy and spectral shape inconsistencies in ground motion sets from spectra-compatibility processes. The system provides ground motion sets by using an input multiparametric selection criterion, driven in progress, to reach the multiparametric consistency of the outputs. In addition, scaling by conserving the spectral target energy allows excluding largely predominant or minority waveforms from the selection; these are usually inserted only as mathematical solutions for compatibility. Therefore, ground motion sets achieving appropriate consistency levels, adequate equivalent energy levels, and spectral assortment are the priority targets over the spectral compatibility process. In this way, the proposed system also presents greater scientific value, in addition to fulfilling requirements from regulations.

The different approach on which based on the proposed method can lead to different questions concerning its reliability as well as its real added value in the panorama of input motion selectors. The answers to these questions have been taken into account throughout the development of the system and are intrinsically linked with its computational structure as well as with the parameters involved in that one. Seismological nature, attenuation, and site soil type control the parameters characterizing the waveforms. Some parametric relationships are statistically present and investigable by the databases' analysis. These natural intercorrelations may be altered by scaling; this effect suggests, even more, the important role of consistency analysis as the driver of the outputs. In this regard, whilst a combined selection coming from multiparametric constrictions is therefore well accepted in the scientific literature (Du et al., 2022; Katsanos et al., 2010), the advantages and importance to promote multiparametric consistency, as well as the explicit meaning of consistency used in the method, have progressively illustrated and deeply discussed in the following sections. Sensitivity analyses will show that combinations of input restriction values increase ground motions plausibility when these parameters are driven to converge to produce consistent outputs. This convergence leads to the inclusion in the ground motion dataset of validated waveshapes that are closer to the expected real ones than the traditional systems.

3. Requirements of the system

The proposed system, encoded in a computer code tool named SHAKER (Seismic Housner intensity As earthquaKE selectoR), is aimed at the selection of a set of natural accelerograms to match the local hazard response spectrum (spectral compatibility). The scaling is functional at energy equalization of signals in terms of Housner Intensity, and a double level of preselection is performed on the seismological and

seismic parameters. The equalization permits to have GMset without signals with large energy predominance, or contrary negligible, introduced only for the spectral matching satisfying. In addition, combining equalization with spectral compatibility admits, instead, that each ground motion has predominance in a spectral sector with respect to the target spectrum. This condition favors a good spectral distribution and assortment. Notwithstanding the key role of equalizing, the core of the system is the multiparametric consistency analysis, which will be in detail in this and other subsequent sections. Hither, main features and capabilities of the procedure can be summarized as follows:

- the earthquake repository is composed by signals with civil engineering significance from the current Italian regional database, ITACA-DB;
- the selection of ground motion sets (GMset) is based on equalizing Housner Intensity, HI; its control input criteria are represented by assigned intervals of magnitude M and epicentral distance D, in a first screening level, and of PGA and scaling factors (SF) in a second screening level;
- different viscous damping ratios of target response spectra can be used, allowing the selection of the relative spectral compatible GMset;
- a statistical consistency analysis of the scaled ground motions, based on the confidence level with respect to the real ground motions contained in the database, is performed in the preselection step;
- the best spectral compatibility combining ground motions results from the screening preselection processes;
- final multiparametric consistency levels about the best spectral compatible GMset are computed.

Its weaknesses, mainly due to the limited extension of the database, are the following:

- Both horizontal and vertical components are considered for scaling and in the selection process. However, only the horizontal components are assumed as target in statistical consistency analyses.
- Only two soil categories – hard and soft soil – are considered in the consistency analysis.

The computational structure is organized into four consecutive computational modules (Fig. 1): i) Local Hazard, ii) Target Spectrum data, iii) Screening & Consistency analyses, and iv) Spectral Compatibility criteria. Each of these modules provides solutions that are employed in the subsequent ones. Therefore, differentiated and independent analyses can be re-run starting from one of the modules and continuing to others.

3.1. Database and site identification

ITACA-DB consists of 4602 elements: 2301 strong motion accelerograms and their associated 5%-damping response spectra. These signals have been collected since 1976 by the Italian National Seismic Network, managed by the National Institute of Geophysics and Volcanology (INGV). ITACA-DB is extracted from the larger ITACA (ITalian ACcelerometric Archive) database (http://itaca.mi.ingv.it/ItacaNet_31/#/home), in which the waveforms are baseline-corrected and processed according to the approach proposed by Paolucci et al., 2011. The selection is made on the horizontal and vertical components (767 records $\times$ 3 components) of records with Peak Ground Acceleration PGA $\geq$ 0.05 g and moment-magnitude $M_w \geq 4.0$; these values are considered valid in the engineering practice. Among the others, some strong motion events contained in the database include: the 2009 L'Aquila Earthquake (M_w = 6.3), the 2012 Emilia Earthquake sequence (M_w = 5.2–6.1), the 2016 Central Italy Earthquake sequence (M_w = 6.0–6.5), the 1980 Irpinia Earthquake (M_w = 6.9), and the 1976 Friuli Earthquake (M_w = 6.0). The PGA of all the listed signals shows long return periods (about 475 years), as defined in the current Italian seismic hazard map developed by INGV (Meletti et al., 2016).

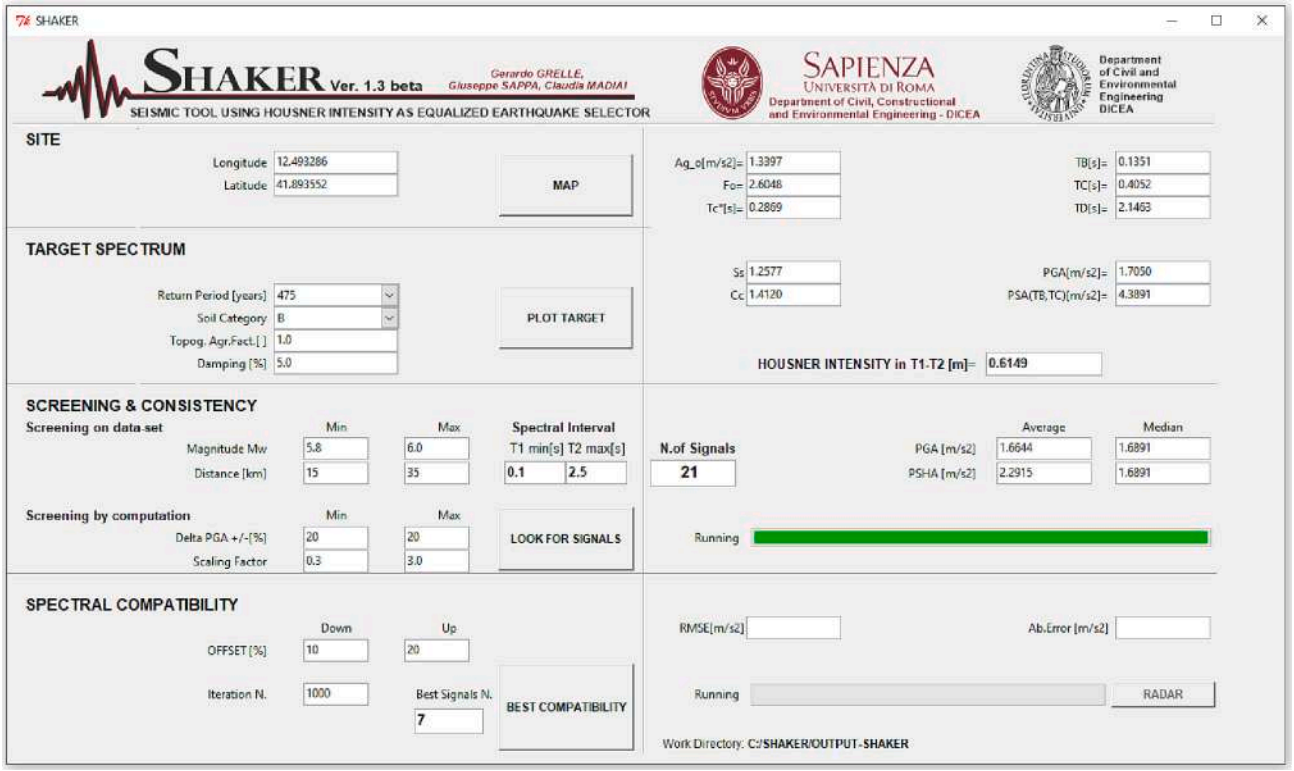

Fig. 1. The architecture of modules composing SHAKER, input parameters at right column, and the corresponding solutions at left column.

Statistical distributions about moment-magnitude, distance, faulting mechanism, and of the subsoil class of the site (based on shear-wave velocity according to NTC-2018) are shown in Fig. 2. Magnitude is mainly between 5.5 and 6.5, while Epicentral Distances mainly range from 0 to 35 km. Subsoil classes C and B are the most frequent ones (65%), in coherence with the shallow soil sequences of the seismogenic zone of the Apennine Chain, characterized by hills and intra-mountain valleys (Falcone et al., 2020; Forte et al., 2019). 21% of the signals have no subsoil classification. Regarding focal mechanisms, 98.8% of the events are associated with Reverse/Thrust and Normal Faulting in equal shares, while a significantly minor part is associated with Strike-slip. In addition, PGA dependence on M-D pairs distribution (Fig. 3) highlights 3D prismatic fields that identified different clustering trends.

The target site to define the seismic hazard is intercepted by coordinates in the UTM reference system (Fig. 4a). Then, maximum bedrock acceleration, a_g, maximum spectral amplification factor, F_o, and normalized period at the end of the constant acceleration branch are the base hazard spectral parameters for the calculation of the return period, T_C*. These parameters are obtained from Annex B of the Italian Building Code (NTC 2008 and 2018) at the four nodes of the mesh, which covers the whole Italian territory, that are closest to the site of interest. The base hazard spectral parameters at the site are computed through spatial interpolation from the values at the four closest nodes. Since the hazard spectral parameters are provided in Annex B for nine standard values of the return period, the parameters for return periods other than those, but included in their intervals, are computed by linear interpolation.

3.2. Target spectrum

The local Target Hazard Response Spectrum (THRS) is computed based on the return period, Tr, and the damping ratio, ξ, according to the simplified approach of the Italian National Building Code (NTC 2018), either on bedrock (Class A subsoil) or soft soil (subsoil of any other class than A). The THRS computation also includes stratigraphic and topographic effects on the spectral shape. As an example, Fig. 4b shows the THRS at a given site for all subsoil classes. Alternatively, response spectra can be inserted manually, such as those obtained from non-simplified approaches as well as advanced seismological hazard studies (e.g. Panza and Bela, 2020) or site response analysis at complex geological sites (e.g. Grelle et al., 2016), or if the analysis is carried out on extra-Italian sites (Amini et al., 2022), without considering the Italian national regulation. Although the use of the proposed system requires a regional dataset, it is possible to run the current version of SHAKER in other seismic areas, provided that their tectonic features are similar to the Italian case. In other words, they must be characterized by extension/compressive orogenic regimes and shallow sources.

3.3. Preselection

The preselection consists of the scaling process to equalize the Housner Intensity and the statistical consistency analysis of the GMset composed by satisfying the input criteria. In a preliminary step, signals are selected from the ITACA database in assigned M and D interval values (screening by database). Pre-computed response spectra with 5%-damping for each of the spectra in the GMSset are used, to compare their spectra with the target spectrum. Since the proposed system runs on different damping ratios, the use of a simplified procedure, based on a metamodel, recomputes these spectra to the assigned damping ratio temporarily, when it is different from 5%. The use of this simplified procedure leads to a significant computational discount in the whole selection process. A further selection, based on assigned interval values of Scaling Factor (SF) and PGA (screening by computation), is subsequently performed for Housner Intensity equalization. Thus, the improvement of accuracy through the physical single-degree-of-freedom SDOF model on a lower number of selected ground motions is achieved. This allows computing correct damped spectra and refining scaling factors.

The aforementioned sequence composing the preselection process (Fig. 5), and the mathematical formulations of parameters brought into play, are explained point by point as follows:

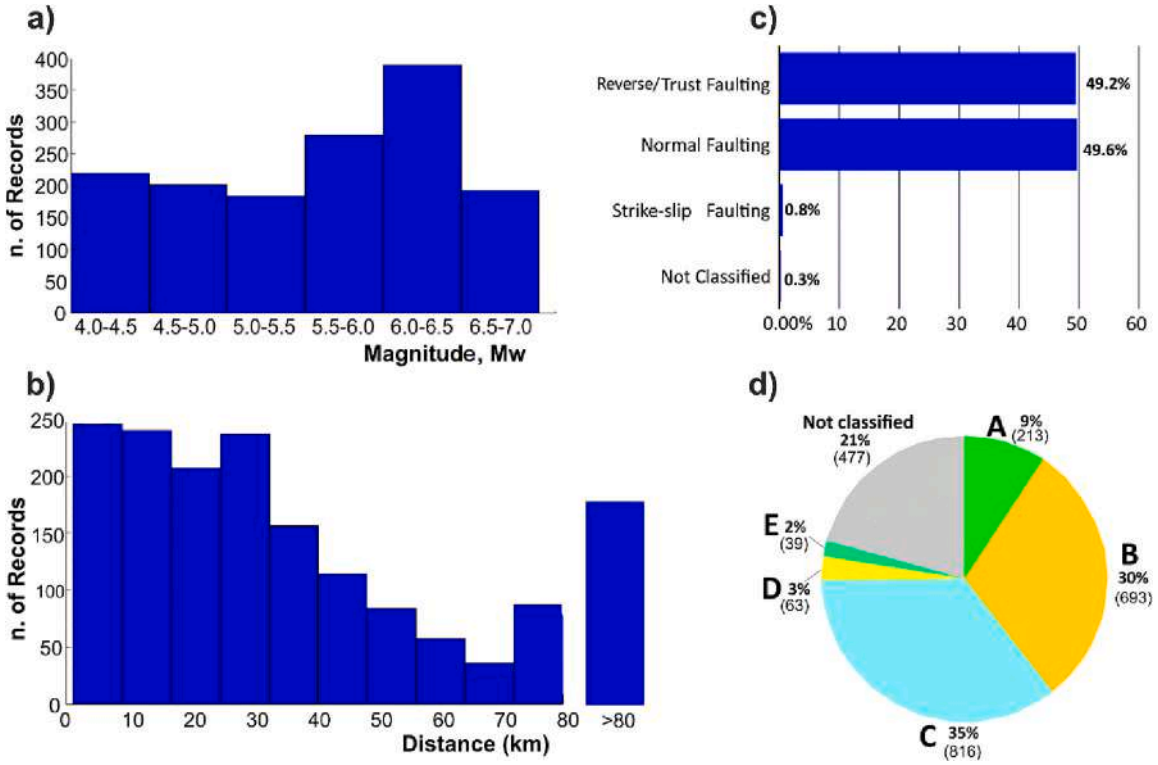

Fig. 2. SHAKER database: a, distribution of Magnitude Moment; b, Epicentral Distance; c, Faulting mechanisms; d, and Subsoil classes according to NTC-2018.

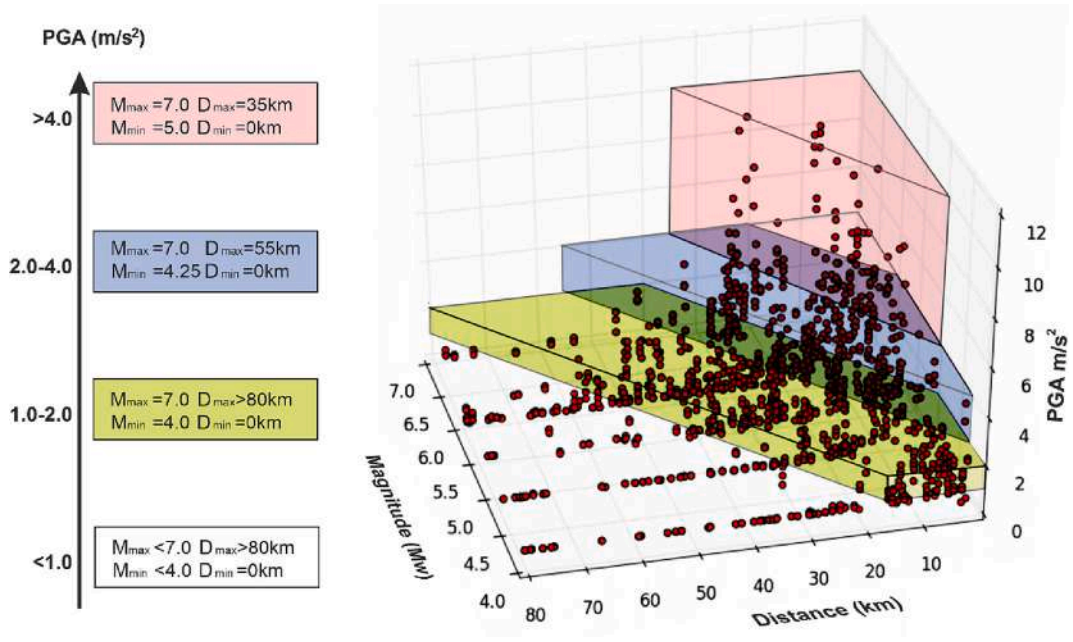

Fig. 3. 3D distribution showing Magnitude-Distance pairs and associated Peak Ground Acceleration (PGA) values. Prismatic fields include the prevalent frequency of M-D pairs for different PGA intervals: 1–2 m/s^2, green prism; 2–4 m/s^2, blue prism; > 4 m/s^2, red prism. (For interpretation of the references to colour in this figure legend, the reader is referred to the web version of this article.)

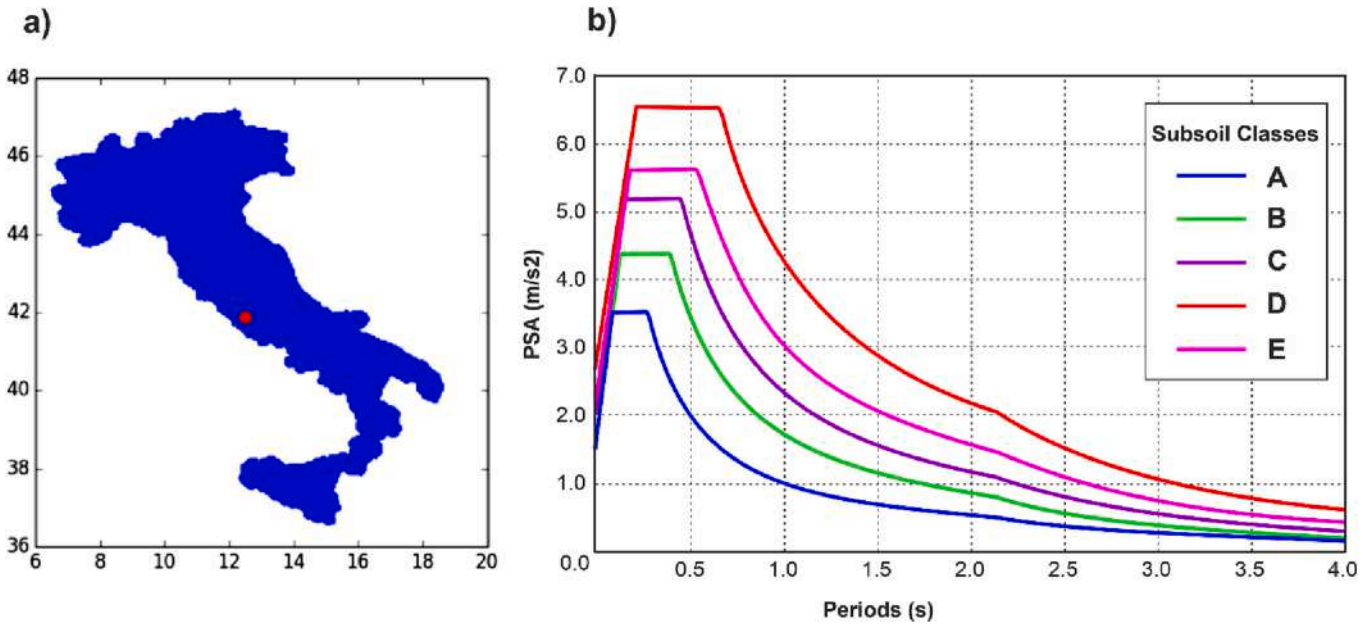

Fig. 4. Example about selection of coordinates: a, local hazard computation; b, Target Hazard Response Spectrum at the selected site including the subsoil classes.

- selection of natural ground motions (GM) and relative response spectra ($PSA_{\xi=5\%}$) in compliance with the assigned M-D interval values;
- recomputing of response spectra PSA if the damping ratio is different from 5% through the following equation (Fig. 6):

$$PSA(\xi_{\neq 0.05}) = DMF \cdot PSA(\xi_{=0.05}) \quad (1)$$

where:

$$DMF = \frac{0.05^{1.3T^{0.7}e^{-T^{1.3}}}}{\xi} \quad (2)$$

it is a non-linear frequency-dependent Damping Modification Factor (sensu Newmark and Hall, 1982) defined by the Gaussian-Weibull exponential function, assuming that the maximum PSA is found at $T = 0.3$ s.

- computation of modified Housner Intensity (HI) for a given spectral interval, T1 to T2. This interval can be different from original formulation, in which 0.1–2.5 s is the integration interval:

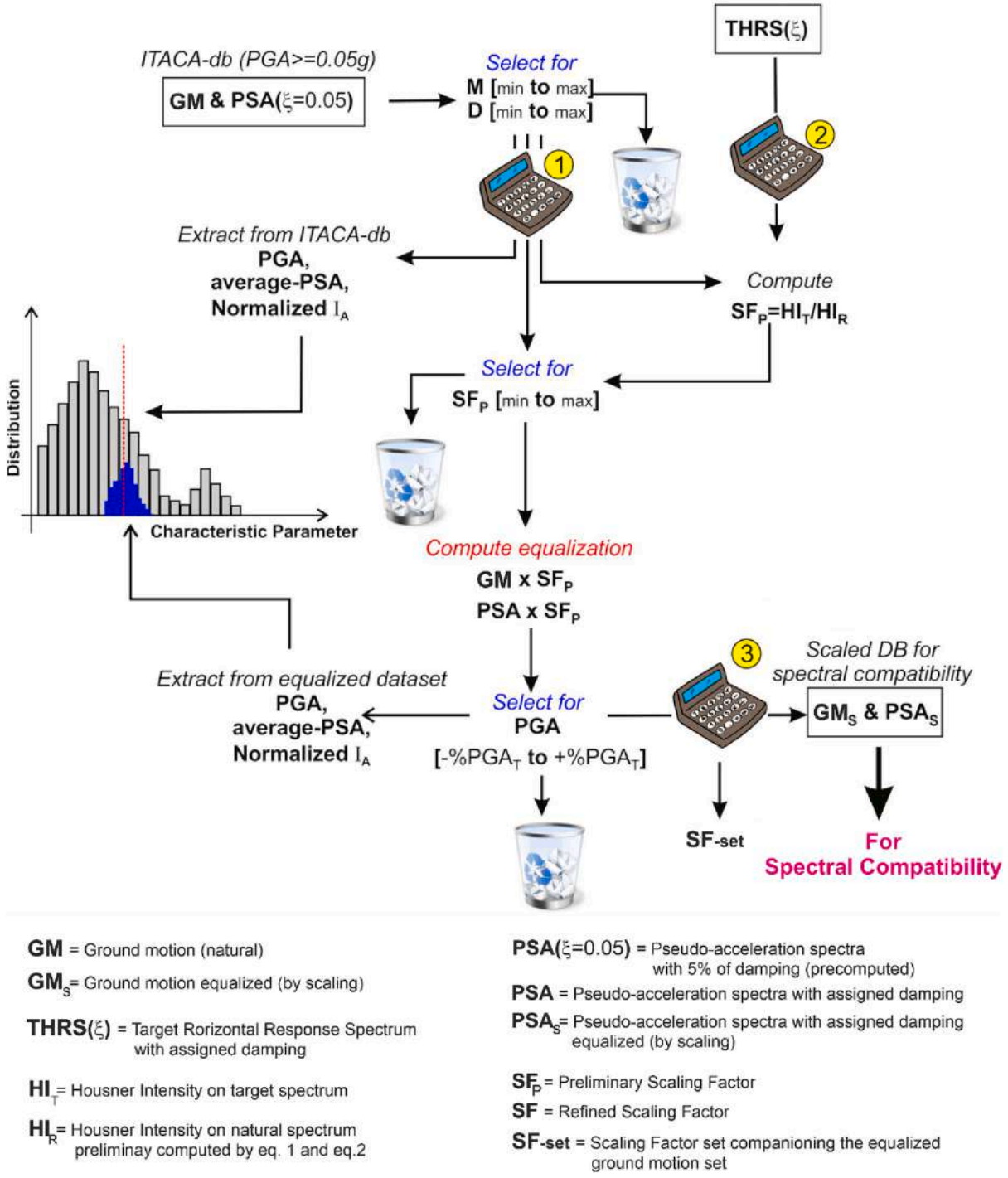

Fig. 5. Flow chart regarding the selection, equalization processes and consistency analysis. Numbered circle 1: solves the eqs. 1, 2, 3 and 5; numbered circle 2 solves the eq. 4; numbered circle 3 solves the SDOF system.

$$HI(\xi,T)=\int_{T1}^{T2} PSV(\xi,T)dT \tag{3}$$

$$SF_P=\frac{HI(\xi,T)_T}{HI(\xi,T)_R}=\frac{\left(\int_{T1}^{T2} PSV(\xi,T)dT\right)_T}{\left(\int_{T1}^{T2} PSV(\xi,T)dT\right)_R} \tag{4}$$

where $PSV(\xi)=\frac{PSA(\xi)}{\omega}$ and $\omega=\frac{2\pi}{T}$ is the angular frequency;

- the calculation of a provisional scaling factor (SF_P) for Housner Intensity equalization:

where subscript "T" is for Target and subscript "R" is for Real (natural ground motion);

- further selection on the equalized GMs that fulfil the PGA and scaling factor (SF)interval values. The PGA interval given by PGA ± ΔPGA is centered on the anchorage value of the target spectrum and Δ is

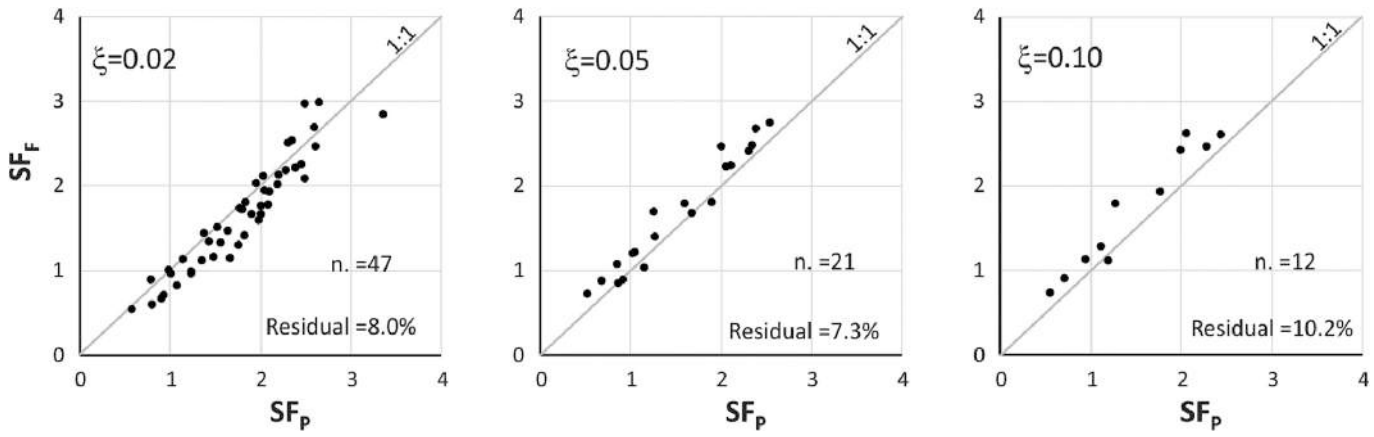

Fig. 6. Comparison between preliminary (SF_P, from the metamodel process) and final (SF_F, from the SDOF system analysis). Residual values are expressed as Normalized Root Mean Square Errors with respect to SF_F. Input data are shown in the Graphic User Interface panel of Fig. 1, except for damping values that are reported in the plots.

expressed in terms of PGA percentage. The selection for the scaling factor is controlled by maximum and minimum limits.

- computation of accurate response spectra by using the single-degree-of-freedom (SDOF). The final scaling factor SFF is then computed.

Reliability performance (Figure6) linked to the preliminary use of fictional damped spectral PSA$\xi \neq 5\%$ computed via DMF (eqs. 1 and 2), is evaluated by comparing the relative preliminary SF (by metamodel) with the refined one SFF (by SDOF). By increasing damping, the number of selectable equalized GMs decreases, since spectral forms, both design (target) and natural ones, are increasingly less close to each other as damping increases.

3.4. Consistency analysis

The consistency of the equalized-GM dataset is defined according to the confidence level captured by the median of the characteristic parameters of signals composing such equalized dataset and the corresponding natural dataset (Fig. 7). This corresponding means that equalized and natural sets insist on the same intervals of magnitude and epicentral distance. Instead, the characteristic parameters are: PGA, Average PSA, PGA to Average-PSA ratio, and Normalized Arias Intensity. The latter is first introduced here and it is defined as the ratio of Arias Intensity to square PGA:

$$I_{APGA} = \frac{\pi}{2g}\int_0^{\infty} (a(t)/PGA)^2 dt. \quad (5)$$

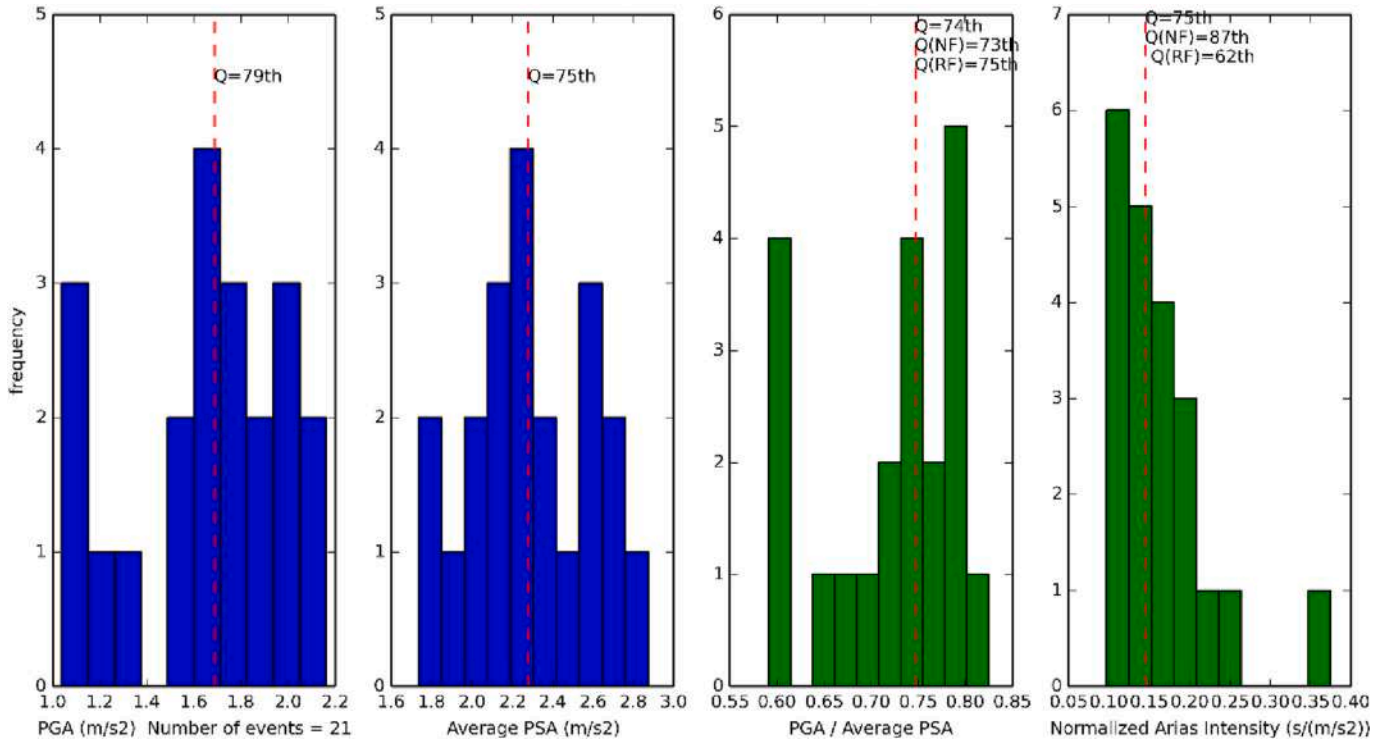

Fig. 7. Example of graphs plotted at the end of module 3 showing, for each characteristic parameter, the percentile confidence levels (Q) intercepted in the ITACA-DB by the median of the equalized GM-set (frequency bar charts); both datasets refer to the same values of M and D intervals. Blue and green bars are respectively the scaled-dependent and the scaled-independent characteristic parameters. Input and output data are in the Graphic User Interface panel of Fig. 1. (For interpretation of the references to colour in this figure legend, the reader is referred to the web version of this article.)

This parameter is expressed in time/g (s3/m), considering that acceleration of gravity is constant, it relates the significant length time of signals making equal the PGA value.

PGA to Average-PSA ratio defines the spectral shape parameter that is not affected by scaling; it is related to representative confidence, thus values falling within the median correspond to the best condition. Usually, high values of this ratio show the presence of spectral peaks at high frequencies (short periods), while low values involve greater amplitude of spectral values at low frequencies (long periods)(D'Amico et al., 2018). The other three parameters define the energy level in spectral and time domains. For these parameters, conservative confidence levels may be taken into consideration. Among these parameters, normalized Arias intensity is scarcely affected by scaling, as PGA and Average PSA have a linear dependence. In addition, to consider the effects related to the focal mechanism, the proposed system reports the confidence levels captured by the medians of the characteristic parameters of the PGA to average PSA ratio and the PGA-normalized Arias intensity, both for Normal Fault NF and Reverse Fault RF. In fact, as previously described, these two parameters are substantially scale-invariant at the same time show significant differences linked to the focal mechanisms. This double analysis is performed only with 5% of damping ratio because spectra with this damping value are precomputed and stored in ITACA-DB.

The consistency analysis can report cases of low affinity between two datasets (equalized and natural), even if both sets refer to the same M-D intervals (Fig. 8). Therefore, it may be hard to choose appropriate input selection criteria to obtain good (or optimized) confidence levels for all four parameters. However, this is facilitated by the fact that the four characteristic parameters are only partially interrelated (e.g. increasing PGA means increasing PSA but not their ratio and not even the length time of the signal). Moreover, the two sets (the equalized set and the corresponding natural) generally have different frequency distributions of the characteristic parameters. As it is well-known, natural datasets are characterized by right-skewed distributions (positive skewness, i.e. increase of density at low values), while pseudo-normal distributions are usually typical of the equalized ones.

In addition, the natural trend of the characteristic parameters affecting consistency suggests assuming short intervals of M-D as selection criteria. In general, the trend of characteristic energy parameters increases with Magnitude and decreases with the distance (attenuation). In this way, the median of the equalized dataset may have a very high confidence level (e.g., above the 95th percentile), when low Magnitude, and/or high distance values, are used. In contrast, ground motions with high Magnitude and short distances have very low representativeness (i.e., below the 25th percentile) when used to match target spectra with low energy levels. This occurs, for example, in the sensitivity analysis shown in Fig. 8. Here, the median PGA of the equalized dataset (consisting of 59 GMs) falls within the 40th in the natural dataset (composed of 231GMs), when an Mw-interval of 5.8–6.2 and a D-interval of 0.00-30 km are used. Instead, when an Mw-interval of 5.5–6.2 and a D-interval of 15-40 km are used, the median PGA of the new equalized dataset (n.24 GMs) increases within the 86th percentile of natural dataset (n. 267 GMs). Both analyses have been performed using the same criteria of SF e ΔPGA (%).

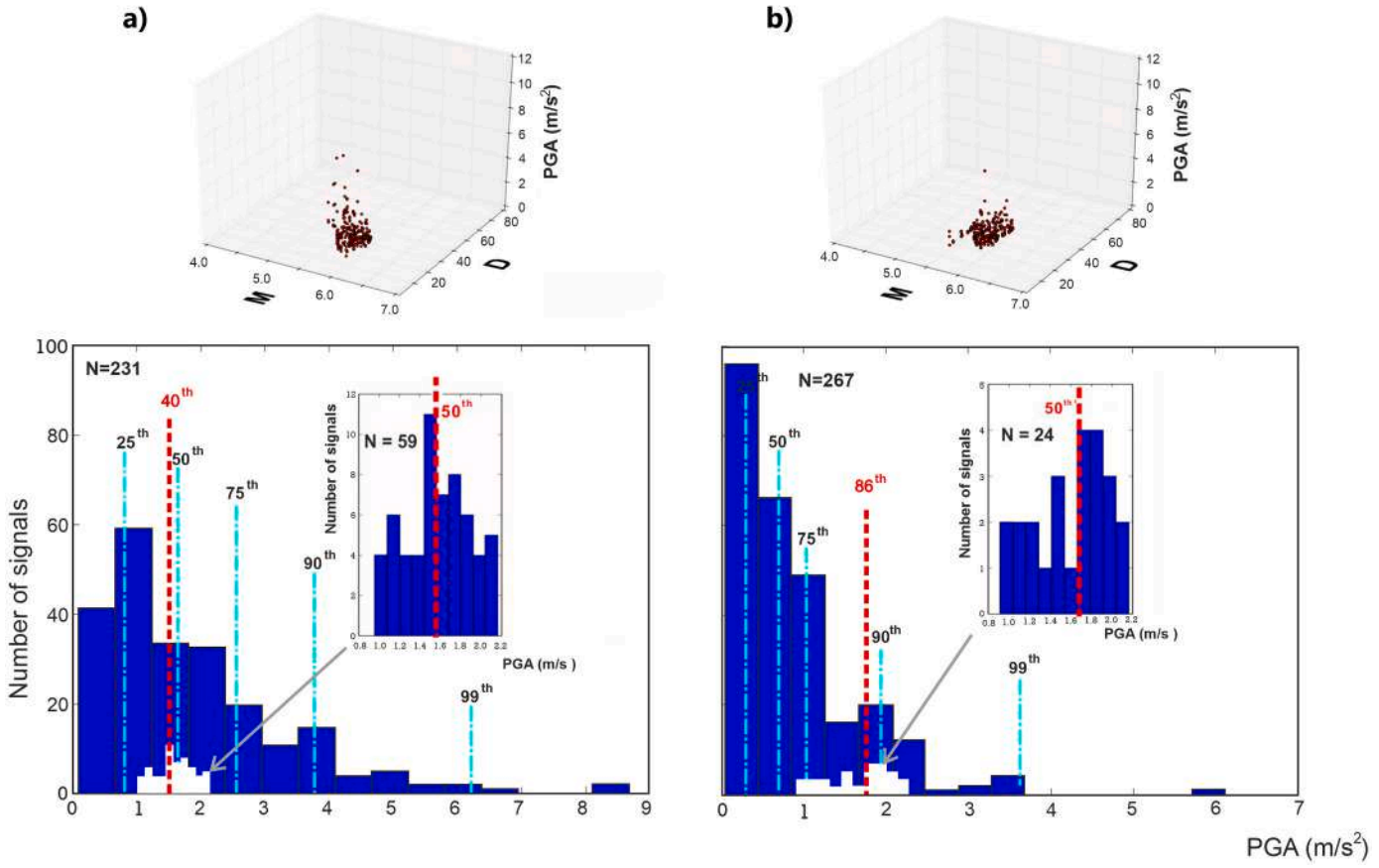

Fig. 8. Example about comparison between confidence percentile levels regarding PGA for two different intervals of Magnitude and epicentral distance: a; Mw = 5.8–6.2 and D = 0.0-30 km, b; Mw = 5.5–6.2 and D = 15-40 km. The distribution of the natural ITACA-DB set is represented by the big bar diagrams while the distribution of the equalized GM dataset is represented by the little bar diagrams; the median of the latter is represented by the red dashed line. Other Input selection criteria are in the Graphic User Interface panel of Fig. 1. (For interpretation of the references to colour in this figure legend, the reader is referred to the web version of this article.)

3.5. Spectral compatibility

In all selector systems, spectral compatibility is chosen as the best match between the average pseudo-acceleration response spectra, $PSA'_j(\xi)$ and $PSA(\xi)$ target, in the spectral interval T1-T2. $PSA'_j(\xi)$ is computed for each element of an assigned number m of ground motions selected within the n equalized and preselected GM-set. The random method is used to combine the relative $PSA_j(\xi)$, while the best performance is associated with the minimum error ε (eqs. 6 and 7) over a fixed number of combinative iterations i. This error was here defined so as to consider both the best average performance, by using the Root Mean Squared Error (RMSE), and by the Max Absolute Error (MAE) to contain slim local peaks. The related expressions are:

$$\varepsilon = \sqrt{(RMSE \bullet \mathrm{MAE})} \tag{6}$$

$$\text{where } RMSE = \sqrt{\frac{1}{n}\sum_{i=1}^{n}\left(PSA'_j\left(\xi, T_{i_{(T1-T2)}}\right) - PSA_T\left(\xi, T_{i_{(T1-T2)}}\right)\right)^2}; PSA'_j = \frac{1}{m}\sum_{j=1}^{m} PSA_j \tag{7}$$

$$\text{and } MAE = max\left|PSA'_j\left(\xi, T_{i_{(T1-T2)}}\right) - PSA_T\left(\xi, T_{i_{(T1-T2)}}\right)\right| \tag{8}$$

A tolerance buffer is set on THRS, to check the acceptability of the matching performance in the T1-T2 period interval. The performance level depends on the number of iterations; anyway, different solutions of equalized ground motion sets may be generated at each iteration round if the number of iterations is relatively low. Thus, the absolute best performance is ensured when many iterations are performed. For example, 10 rounds of 1000 iterations each have been performed to build a compatibility set of 7 GMs. Ten sets fulfill spectral compatibility and a total number of different 15 GMs were selected, only 4 of these are present 9 times out of 10. In this case, a number >2000 iterations assures the best match (Fig. 9).

It can be easily understood that the performance quality depends on the numerosity n, of the equalized GMset, as well as on the number of iterations i that is used, and on the number of the equalized GMs, m (Fig. 10). Generally, the goodness of the performances increases along the number of iterations, i. A non-monotonic behavior in the performance quality is associated with m. Instead, the sensitivity analyses suggest that good matching performances are achieved (with offsets) if the ratio between n and m is >2.5–3.0. Therefore, it may be necessary to perform new preselection rounds to include more equalized signals n, by extending all, some, or only one of the input criteria intervals.

A radar chart at the end of the spectral compatibility process summarizes the general confidence level about the characteristic parameters of signals constituting the spectral compatibility GMset (Fig. 11). The confidence levels of the four characteristic parameters for each GM of the compatible set and their median are plotted in the diagram. In addition, rhomboidal sectors define the adequate confidence and representativeness levels of the characteristic parameters in terms of spectral energy and shape, respectively. Concerning spectral energy, a confidence level is considered adequately conservative if the median value falls within the interval of the 60th–90th percentile (sector IV). Above this interval, the values are considered excessively conservative (sector V); below it, confidence levels are non-conservative or not very conservative (sector III). An interval of the 25th–75th percentile has been used to define the representativeness of the spectral shape ratio (sector I). Based on these intervals, a rhomboid sector, defining

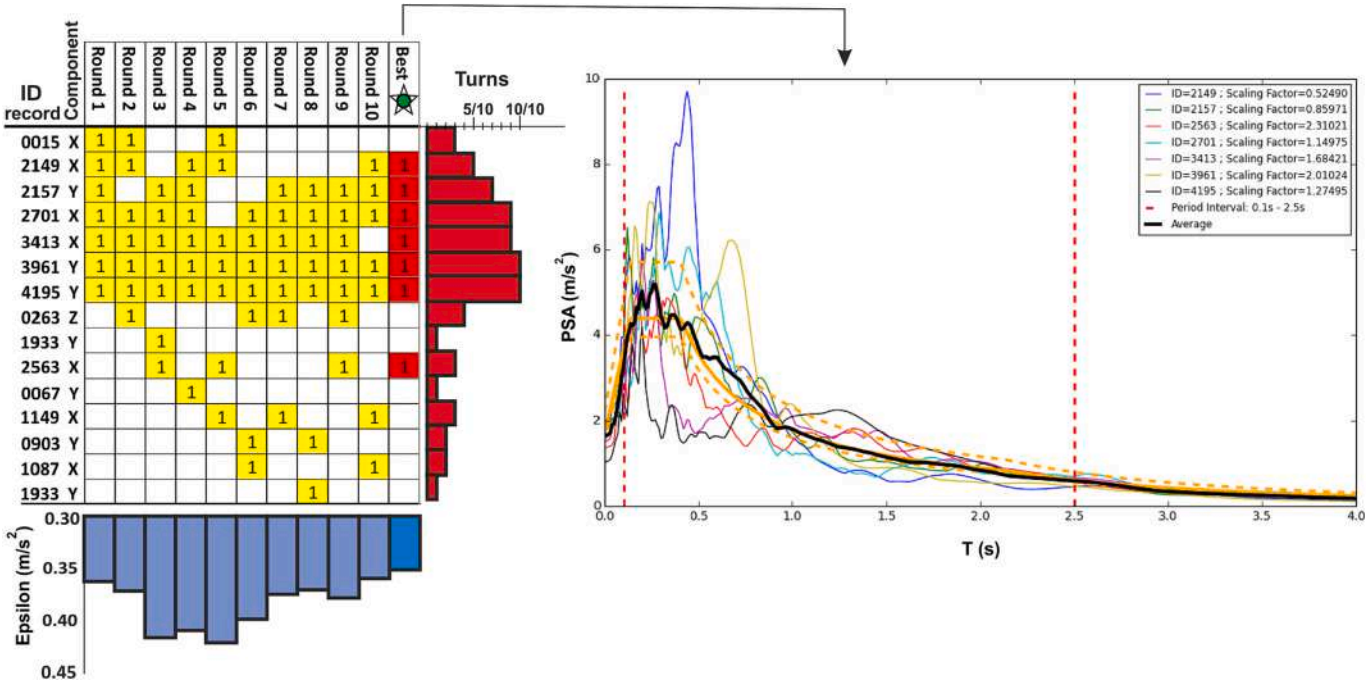

Fig. 9. Compatibility process performed by module 4 and relative frequency analysis of 10 rounds, 1000 iterations each; the additional best performance was ensured by performing 5000 iterations. Input values are set as in the GUI panel of Fig. 1.

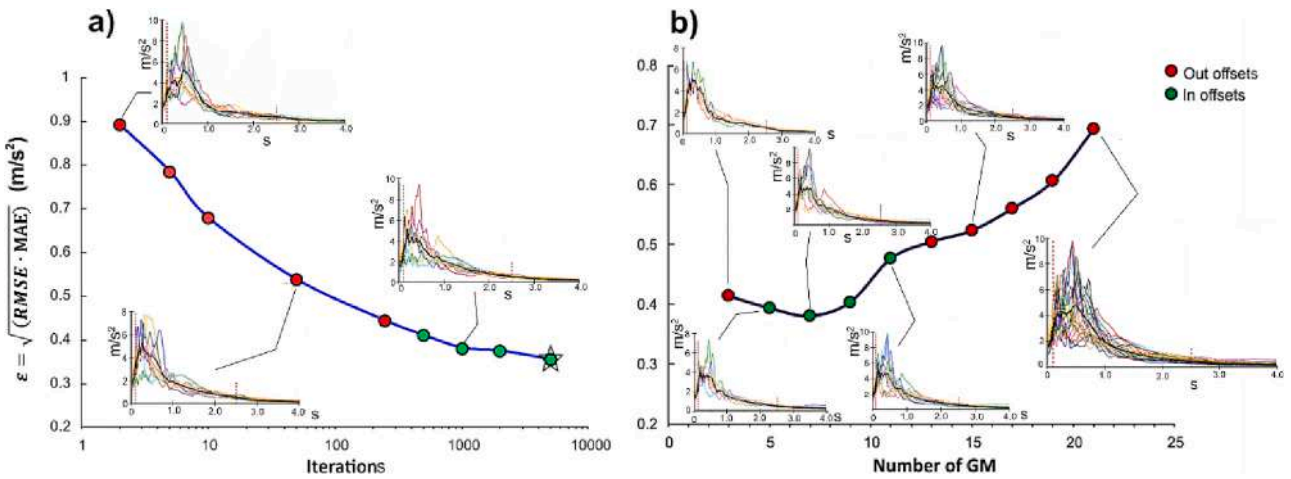

Fig. 10. Example about matching performance of the compatible equalized GMs: a, versus number of iterations;b, versus number of equalized GMs used to build the spectral compatibility set. Input values are set as in the GUI panel of Fig. 1.

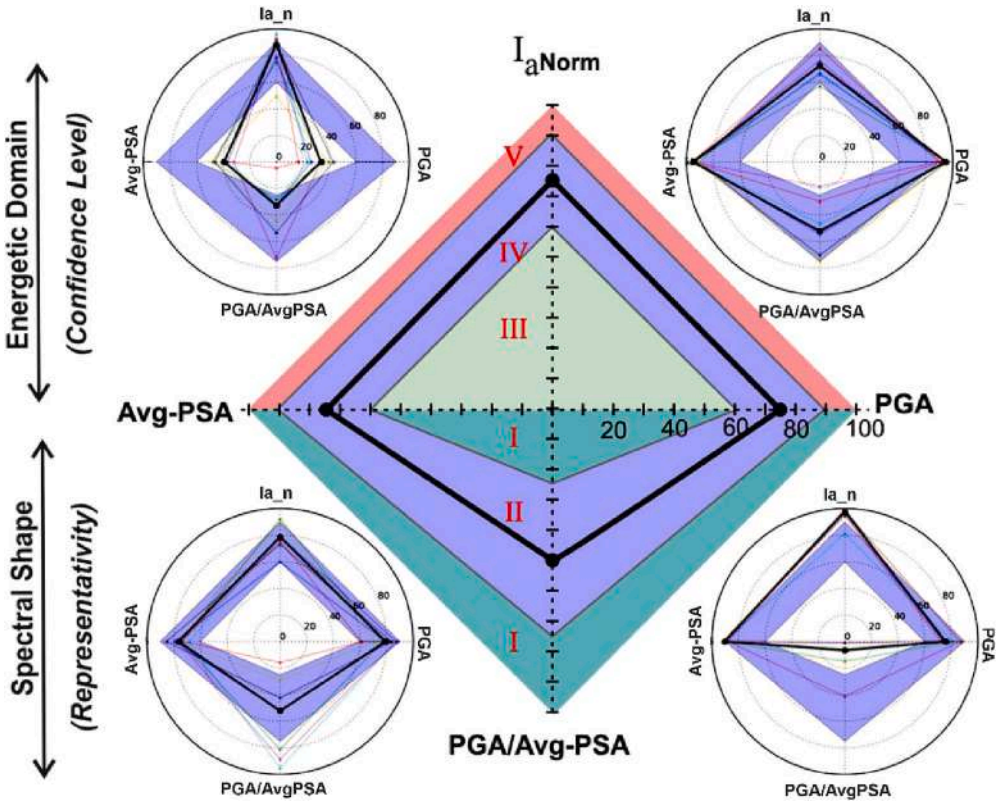

Fig. 11. Radar diagram of consistency. Sector: I, low representativeness; II, good representativeness; III, low confidence level (low-conservative); IV, adequate confidence level (conservative); V, very high confidence level (excessively conservative). Radar plots: 1, consistent equalized-set; 2, inconsistent equalized-set stemming from excessive up-scaling and use of far events; 3, inconsistent equalized stemming from excessive down-scaling and use of close events; 4, inconsistent equalized-set due to high discrepancy between the spectrum target and chosen Magnitude and distance intervals, combined with decentralized SF and %ΔPGA intervals.

consistency, was plotted in the radar graph. The consistency of the solution is represented by a median with a regular shape falling within that rhomboid sector. Conversely, a horizontal stretching generally involves a vertical shortening of the rhomboid and vice versa. In such cases, a more adequate interval of the computational screening parameters ΔPGA(%) and SF are required. Conversely, an uncentered rhomboid median suggests the need to modify the distance and/or Magnitude interval values. Applicative examples of sensitivity to consistency analysis are discussed in paragraph 5.1.

4. Parametric relationship

4.1. Soil typology

Ground motion records on stiff-soil (rock) sites have substantial spectral differences from soft-soil ones. A common opinion is that the input spectra must be selected considering the lithology of origin when they are used to represent the expected hazard at the bedrock below soft sequences (class A subsoil) (Corigliano et al., 2012). This subject is crucial when site ground response and co-seismic geotechnical instabilities must be assessed. Specifically, the stiff/soft-soil promiscuity in ground motion database sources can result in a significant energy gap between the selected ground motions, mainly with short periods of

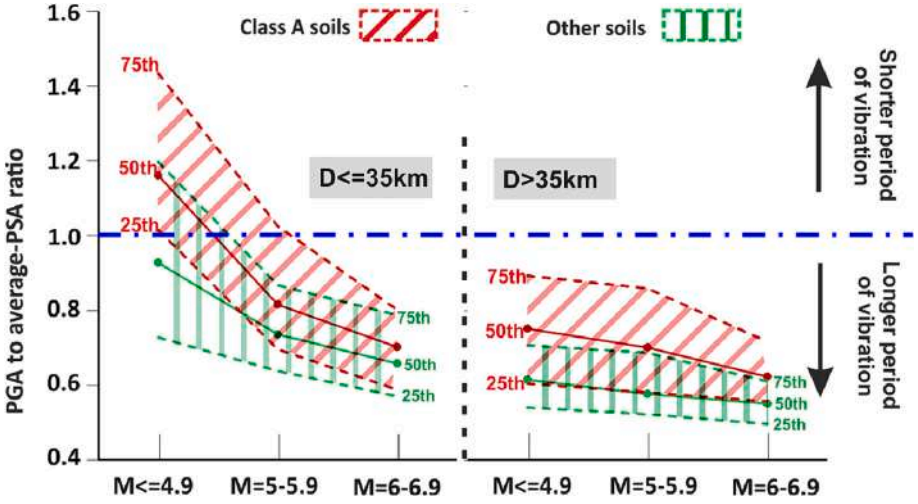

Fig. 12. Trend of PGA to average-PSA ratio for stiff (class A) and soft soils as a function of epicentral distance (D) and Magnitude (M) for ITACA-DB ground motions.

vibrations (Laurendeau et al., 2013). This effect leads to higher spectral shape values, PGA to average-PSA ratio, for outcropping rock sites, compared to soft soil sites (Fig. 12). Concerning ITACA-DB, with reference to three Magnitude intervals ($M \leq 4.9$; $5 \leq M \leq 5.9$; $6 \leq M \leq 6.9$) the median values of this ratio for GMs on subsoil class A are always greater than those recorded on other soft subsoil categories. The gap increases with the distance for $M \geq 5$ and decreases with Magnitude regardless of distance. The distant-dependent effect is due to the amplitude-selective soil damping, which strongly reduces the propagation of short wavelengths. The Magnitude-dependent can be explained through the greater energy released at lower frequencies with the extension of the fault failure surface.

4.2. Focal mechanisms

In ITACA-DB, the number of Normal Fault records is very close to the one of Reverse Fault records, so this provides a good comparison for some parametric trends linked with these two failure regimes (Fig. 13). As highlighted by the PGA distribution regarding Magnitude and epicentral distance, the signals produced by the Reverse Faults related to a lower number of events encompass fewer Magnitude classes than the Normal Fault ones. Therefore, the high number of these signals explains that the signals linked to Reverse Faults have lower distance-dependent attenuation than the ones with Normal Faults. This effect is made more evident by the presence of a higher number of signals of Reverse Faults at long epicentral distances, than ones coming from Normal Faults. In the considered database, there are few signals associated with the latter mechanisms for $D > 30$–40 km and $M < 5.5$. Furthermore, for short epicentral distances, Normal Fault events show higher PGA values than Reverse Fault events and decrease more rapidly with the distance, for the same Magnitude interval. These trends may be due to amplitude-selective damping related to the wavelength (periods), as indirectly confirmed by the PGA to average-PSA ratio distributions. The signals produced by Reverse Faults sources have a more even energy distribution in the spectral domain than the Normal ones, as suggested by the lower values of previously mentioned ratio by comparing the firsts with the seconds. Conversely, the signals produced by Normal Faults are more concentrated in short periods of vibration associated with higher PGA values and so with higher PGA to average-PSA ratio. The median of the PGA to average-PSA ratio distribution is 0.8 for GMs from Normal Faults and 0.6 for Reverse Faults. The difference in the effects produced by ground motions having similar PGA and different spectral energy is well known as regards both civil structures (Tao et al., 2019; Chang et al., 2021) and ground instability phenomena such as landslides (Jibson and Tanyaş, 2020) and soil liquefaction (Castro et al., 1983; Nong et al., 2020).

Focal mechanism effects are evident also in the time domain by considering the Arias Intensity, I_A, in its normalized formulation, $I_{A\text{-}PGA}$, shown in eq. (5). This parameter shows (Fig. 13) that signals produced by Normal Faults have on average significantly smaller $I_{A\text{-}PGA}$ values than those produced by Reverse Faults. This different effect on the time length of signals is caused by the combination of different spectral effects due to focal mechanisms and amplitude-selective damping, which depend on the wavelength during propagation. The time length of the input ground motions has recently taken a significant role in civil engineering design. (Bhanu et al., 2021; Chandramohan et al., 2014; Du et al., 2020; Sun et al., 2018). Parameters that take into account the duration have started to be employed in hazard assessing, because this is crucial when plastic cyclic cumulative deformations control the seismic performance as it occurs in geotechnical and natural systems, such as earth dams and slopes (Grelle et al., 2011; Grelle and Guadagno, 2013; Nakamura et al., 2014; Nettles and Ekström, 2004; Wang et al., 2015; Zhang et al., 2013), and in soil densification and liquefaction effects (Blázquez and López-Querol, 2006; Liu et al., 2001).

5. Reliability and discussion

5.1. Sensitivity analysis for a consistent selection

In the equalized GM-set preselection, an appropriate choice of the input criteria is necessary for obtaining a good consistency level of the compatible GM-set. To illustrate this statement, multiparametric calibration procedures have been performed on three sites, with different seismic hazard levels. For these sites, the local hazards (Fig. 14) come from the disaggregate analysis of national seismic hazards carried out by INGV (Barani et al., 2009). The sites are assumed to have a flat morphology and are located in the cities of Turin, Rome, and Reggio Calabria. The expected hazard is defined in terms of PGA with an exceedance probability of 10% in 50 years (return period of 475 years) with a B subsoil class. In this regard, Turin is characterized by far-field seismicity with events from low to low-medium Magnitude (4.0–5.4) and long distances (15–45 km). Rome is characterized by near-field seismicity with events from low to low-medium Magnitude (4.0–5.4) and short distances (0.0–10 km). Finally, Reggio Calabria is characterized by near-field seismicity and events with Magnitudes from medium to high (4.8–7.0) at short distances (0.0–10 km).

Consistency analysis is aimed at the preselection of highly consistent ground motion sets of at least 21 signals, which ensure spectral compatibility for 7 of them. This set was built by interactive progressive running to reach adequate confidence levels for the characteristic

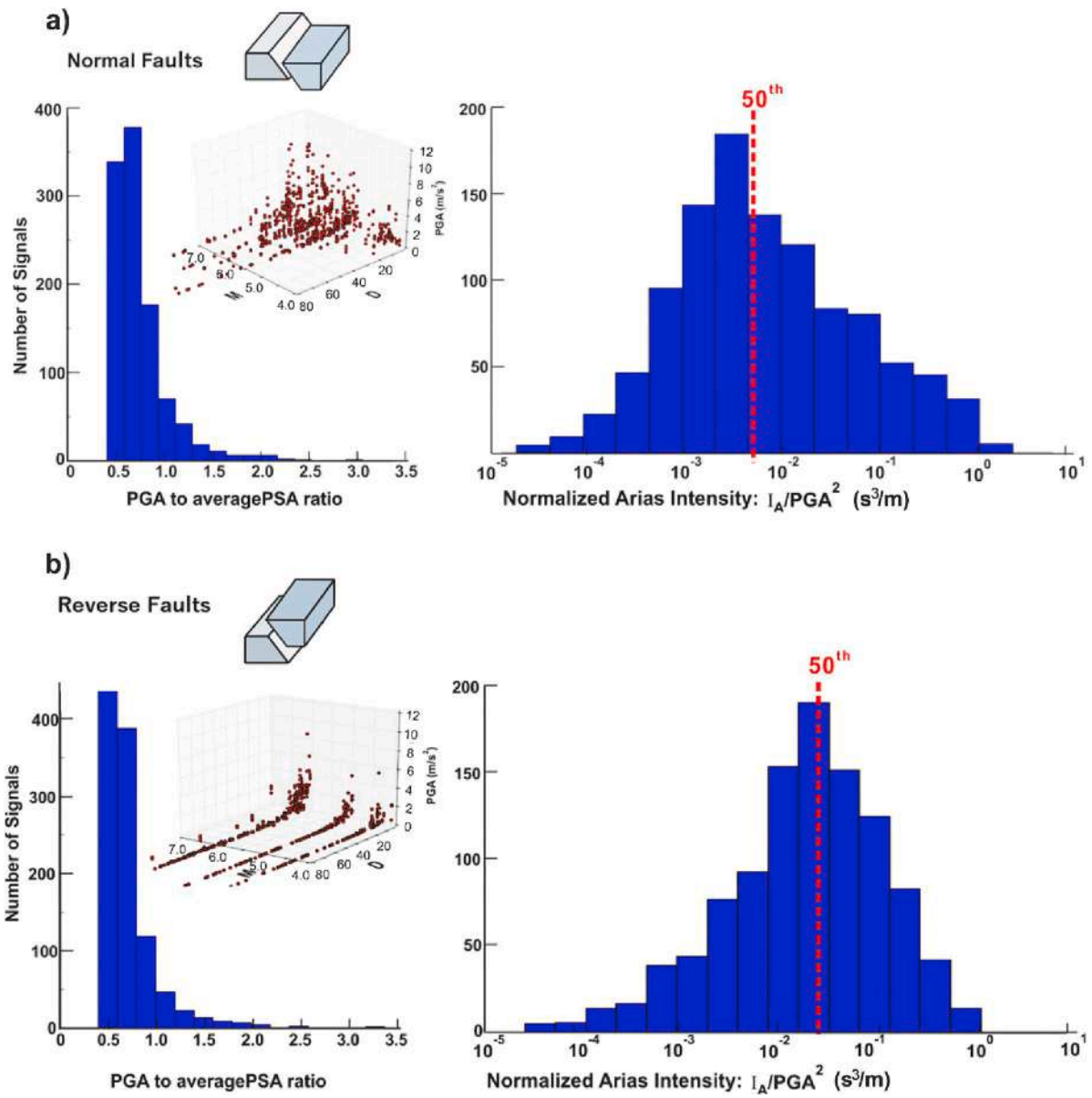

Fig. 13. Spectral shape and energy distribution in relation to the main focal mechanisms: a, Normal Fault; b, Reverse Fault.

parameters. This running starts to assume the Magnitude-Distance pairs from the expected local hazard, while default scaling factor interval equal to 0.3–3.0 and an initial ΔPGA(%) = ±20% are used. For all sites, an interval of 0.15–2.0 s is chosen to match the spectral compatibility.

Progressive output concerning sensitivity to multiparametric calibration in the preselection step is reported in Fig. 15, showing consistency between seismological hazard parameters (initially imposed by M and D pairs), spectral energy (imposed by target spectrum), and spectral shape of the equalized GMset addressed to spectral compatibility fit. The site in Turin shows low consistency by selecting initial hazard M and D intervals of 4.0–5.4 and 15–45 km, respectively. The highest consistency appears for a smaller Magnitude interval, 4.8–6.0, centered at a distance of 30 km. Concerning the site in Rome, the spectral energy associated with the target hazard spectrum has a low consistency with the initial hazard M and D intervals. Because considering these intervals, very low values of PGA to average-PSA ratio result (spectral shape) are associated with extremely conservative values of Arias Intensity. Over eight rounds were required to find an M-D interval pair to fulfil good consistency levels. A larger GMset is obtained when applying the selection criteria of Magnitude up to 5.9 and distances above 10 km. Concerning the site in Reggio Calabria, local hazard studies suggest a large interval of Magnitude with a short interval of distance, respectively of 4.8–7.0 and 0.0–10 km. Using these initial criteria, the equalized GMset appears to be scarcely representative in spectral shape, with highly conservative values of the other characteristic energy parameters. This condition suggests that the spectral energy associated with the target spectrum is inappropriate if the matching derives by scaling signals with low values of Magnitude. In this case, the representativeness level of the spectral shape increases when the magnitude interval comprises values over 5.5. In addition, the distance interval needs to be above 15 km, to include a larger number of signals fulfilling the number required for adequate spectral compatibility.

Concerning focal mechanisms, the consistency analysis reports higher representativeness for the GMs from Reverse Faults, compared to those from the Normal ones, if natural GMs are equalized to match the design target spectrum proposed by the national building code. In general, concerning focal mechanisms and the design spectra proposed by the national building code, the consistency analysis reports higher representativeness for the GMs from Reverse Faults, compared to those from the Normal ones. As discussed in the previous paragraph, this

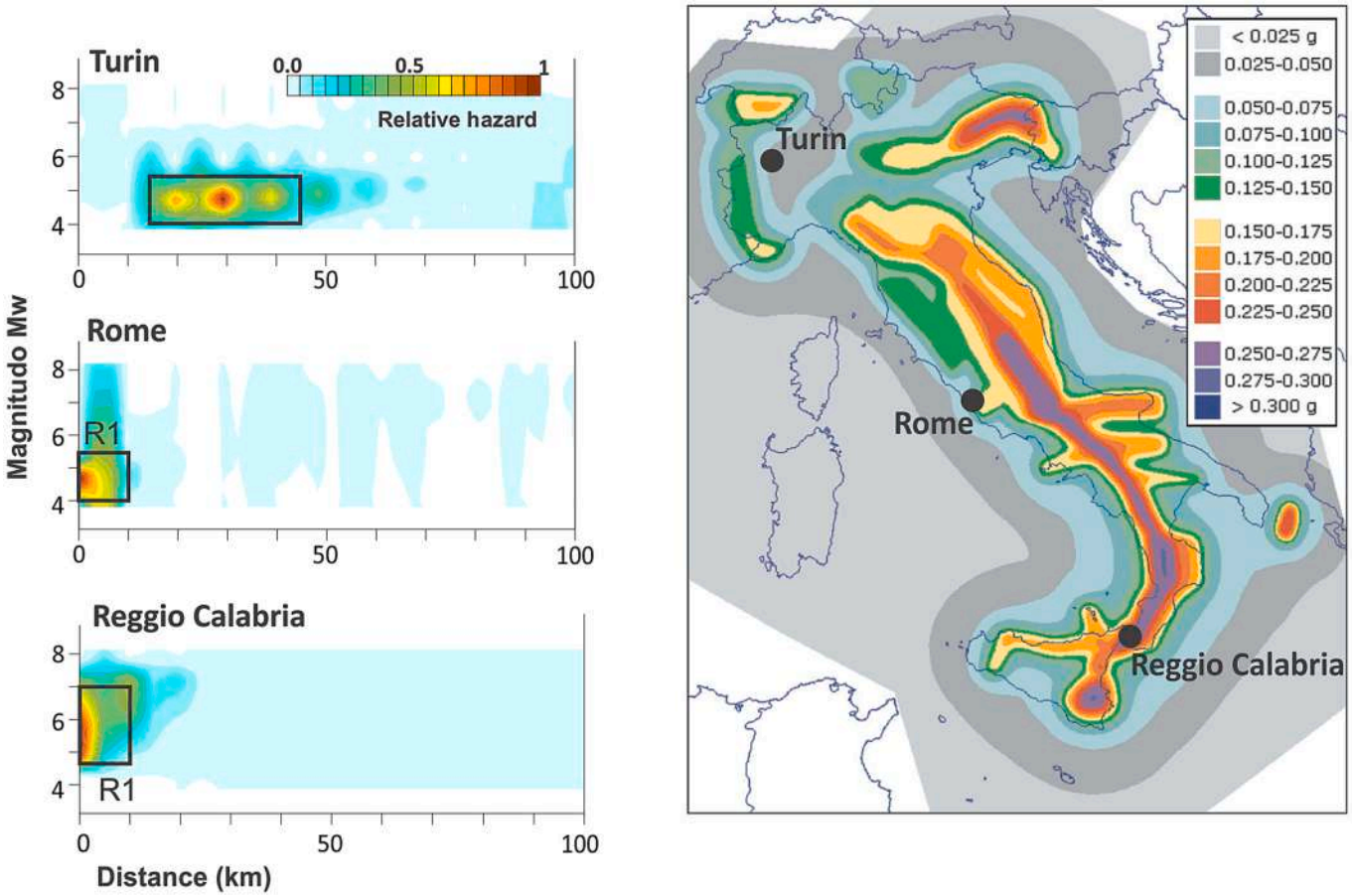

Fig. 14. Local hazard at three sites with different types and levels of expected seismicity. PGA values are associated with an exceedance probability of 10% in 50 years (return period of 475 years) on outcropping bedrock (soil class A). Relative hazard in colour bar expresses the hazard probability distribution, normalized to the maximum value.

tendency occurs because the equalized GMs coming from Reverse Faults keep more energy at long periods than the GMs from Normal Faults. Consequently, spectra from reverse faults are more similar to the target spectrum also in terms of PGA to Average PSA ratio. On the other hand, the energy process equalization entails higher values of the scaling factor and, consequently, of scaled PGA for GMs coming from Normal Faults. In this way, PGA values are more subject to falling out of the threshold initially assumed as selection criteria. This effect seems to be inverted at low magnitudes and small distances, as in the case of the site in Rome, where greater representativeness was found for GMs from Normal Faults than from the Reverse ones.

Finally, a quality-quantitative comparative analysis was performed concerning expected consistency level and spectral compatibility match of the ground motion set (Fig. 16). Certainly, concerning input criteria, large intervals of Magnitude and/or distances easily ensure spectral compatibility, but at the same time this tends to push the relative characteristic parameters toward the limits of the confidence levels and so of the consistency. This generally occurs for high confidence levels of spectral energy parameters, (PGA, avg-PSA and normalized Arias intensity $I_{A\text{-}PGA}$) associated with very low representativeness, showed by a low confidence level of PGA to Average PSA ratio, such as in the example of Turin and Reggio Calabria at the first round. On the other hand, a small interval of Magnitude and distance may not ensure an adequate number of equalized signals to satisfy spectral compatibility. Therefore, the aforementioned intervals should be changed; moreover, an attempt should be made to increase the intervals of ΔPGA and scaling factor, SF, as in the case of the site in Rome.

5.2. Comparative analysis

A comparative analysis with the recently upgraded web-Rexel selector (Iervolino et al., 2010; Sgobba et al., 2019) highlights the progress introduced by the selector SHAKER here proposed. The comparison is performed on a near-field stress test, contextualized in the well-known seismic condition of Amatrice town, which has recently been involved in the seismic sequence of Central Italy (2016–2017) (Grelle et al., 2020). The activation of the nearby Monte Vettore Normal Fault and the released Magnitude are hazard-expected events with a return period of 475 years. The main event was recorded by accelerometric station AMT located on a topographical relief, highly enhancing amplificative effects (Grelle et al., 2021). The horizontal design elastic spectrum with 5% of damping regarding the aforesaid hazard expected event is the target in the comparative analysis. A topographic amplification coefficient of 1.4 was used, as defined in the NTC 2018 for such cases. Moreover, input selection criteria of Magnitude interval equal to 5.8–6.5 and epicentral distance <10 km, are assumed from both systems. The term of comparison is an output ground motion set composed of 7 signals, which is compatible with the target spectrum in the interval 0.15–1.40s.

In SHAKER, further input parameters regarding the intervals of ΔPGA and scaling factor thresholds have to be set, based on the consistency analysis in the preselection step. Considering the near-field scenario, high PGA values are expected. For this reason, the following assumptions are made in the first preselection round: the unlimited increase of this parameter (e.g. imposing ΔPGA 1000%) and an IF threshold of 3.0. This round produced a series of 63 signals, selected by

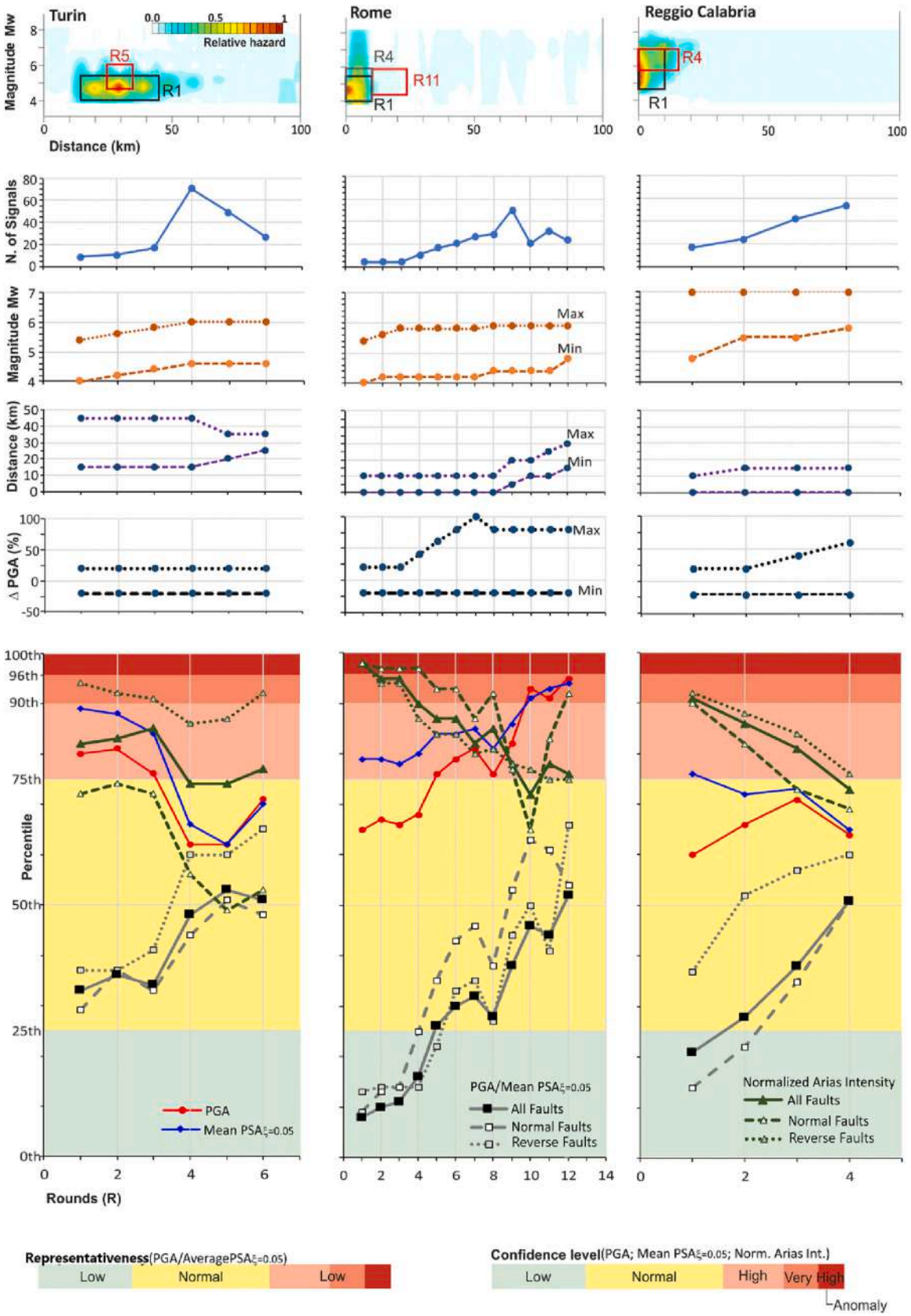

Fig. 15. Consistency analysis of the sites is reported in Fig. 14. Representativeness and confidence levels are reported in the two-colour bar scales below. Boxes in the hazard distribution regard coupled values of Magnitude and distance seeming from the computational rounds regarding the initial (black) and best consistency (red) of M-D coupled values. (For interpretation of the references to colour in this figure legend, the reader is referred to the web version of this article.)

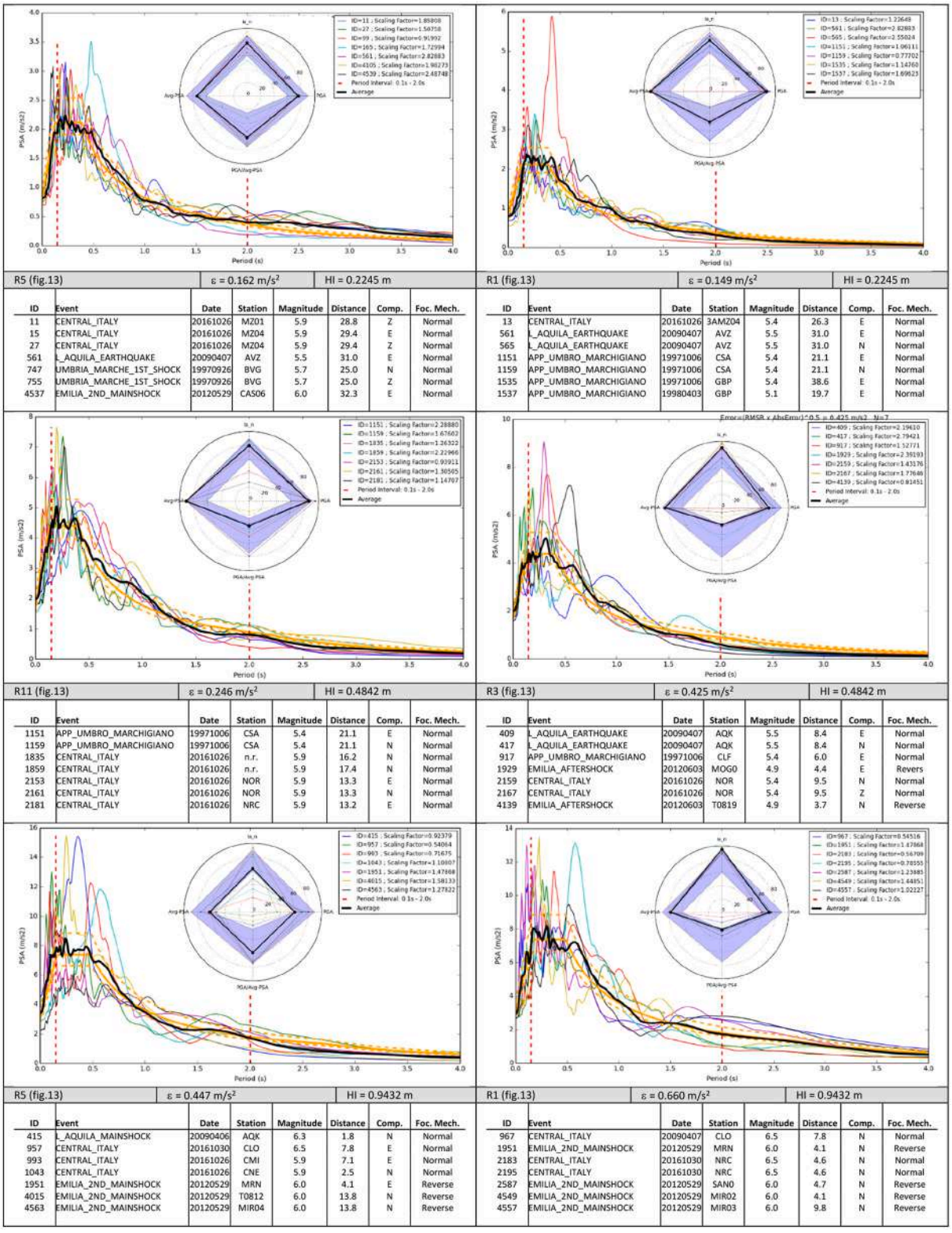

ID	Event	Date	Station	Magnitude	Distance	Comp.	Foc. Mech.
11	CENTRAL_ITALY	20161026	MZ01	5.9	28.8	Z	Normal
15	CENTRAL_ITALY	20161026	MZ04	5.9	29.4	E	Normal
27	CENTRAL_ITALY	20161026	MZ04	5.9	29.4	Z	Normal
561	L_AQUILA_EARTHQUAKE	20090407	AVZ	5.5	31.0	E	Normal
747	UMBRIA_MARCHE_1ST_SHOCK	19970926	BVG	5.7	25.0	N	Normal
755	UMBRIA_MARCHE_1ST_SHOCK	19970926	BVG	5.7	25.0	Z	Normal
4537	EMILIA_2ND_MAINSHOCK	20120529	CAS06	6.0	32.3	E	Normal

ID	Event	Date	Station	Magnitude	Distance	Comp.	Foc. Mech.
13	CENTRAL_ITALY	20161026	3AMZ04	5.4	26.3	E	Normal
561	L_AQUILA_EARTHQUAKE	20090407	AVZ	5.5	31.0	E	Normal
565	L_AQUILA_EARTHQUAKE	20090407	AVZ	5.5	31.0	N	Normal
1151	APP_UMBRO_MARCHIGIANO	19971006	CSA	5.4	21.1	E	Normal
1159	APP_UMBRO_MARCHIGIANO	19971006	CSA	5.4	21.1	N	Normal
1535	APP_UMBRO_MARCHIGIANO	19971006	GBP	5.4	38.6	E	Normal
1537	APP_UMBRO_MARCHIGIANO	19980403	GBP	5.1	19.7	E	Normal

ID	Event	Date	Station	Magnitude	Distance	Comp.	Foc. Mech.
1151	APP_UMBRO_MARCHIGIANO	19971006	CSA	5.4	21.1	E	Normal
1159	APP_UMBRO_MARCHIGIANO	19971006	CSA	5.4	21.1	N	Normal
1835	CENTRAL_ITALY	20161026	n.r.	5.9	16.2	N	Normal
1859	CENTRAL_ITALY	20161026	n.r.	5.9	17.4	N	Normal
2153	CENTRAL_ITALY	20161026	NOR	5.9	13.3	E	Normal
2161	CENTRAL_ITALY	20161026	NOR	5.9	13.3	N	Normal
2181	CENTRAL_ITALY	20161026	NRC	5.9	13.2	E	Normal

ID	Event	Date	Station	Magnitude	Distance	Comp.	Foc. Mech.
409	L_AQUILA_EARTHQUAKE	20090407	AQK	5.5	8.4	E	Normal
417	L_AQUILA_EARTHQUAKE	20090407	AQK	5.5	8.4	N	Normal
917	APP_UMBRO_MARCHIGIANO	19971006	CLF	5.4	6.0	E	Normal
1929	EMILIA_AFTERSHOCK	20120603	MOG0	4.9	4.4	E	Revers
2159	CENTRAL_ITALY	20161026	NOR	5.4	9.5	N	Normal
2167	CENTRAL_ITALY	20161026	NOR	5.4	9.5	Z	Normal
4139	EMILIA_AFTERSHOCK	20120603	T0819	4.9	3.7	N	Reverse

ID	Event	Date	Station	Magnitude	Distance	Comp.	Foc. Mech.
415	L_AQUILA_MAINSHOCK	20090406	AQK	6.3	1.8	N	Normal
957	CENTRAL_ITALY	20161030	CLO	6.5	7.8	E	Normal
993	CENTRAL_ITALY	20161026	CMI	5.9	7.1	E	Normal
1043	CENTRAL_ITALY	20161026	CNE	5.9	2.5	N	Normal
1951	EMILIA_2ND_MAINSHOCK	20120529	MRN	6.0	4.1	E	Reverse
4015	EMILIA_2ND_MAINSHOCK	20120529	T0812	6.0	13.8	N	Reverse
4563	EMILIA_2ND_MAINSHOCK	20120529	MIR04	6.0	13.8	N	Reverse

ID	Event	Date	Station	Magnitude	Distance	Comp.	Foc. Mech.
967	CENTRAL_ITALY	20090407	CLO	6.5	7.8	N	Normal
1951	EMILIA_2ND_MAINSHOCK	20120529	MRN	6.0	4.1	N	Reverse
2183	CENTRAL_ITALY	20161030	NRC	6.5	4.6	N	Normal
2195	CENTRAL_ITALY	20161030	NRC	6.5	4.6	N	Normal
2587	EMILIA_2ND_MAINSHOCK	20120529	SAN0	6.0	4.7	N	Reverse
4549	EMILIA_2ND_MAINSHOCK	20120529	MIR02	6.0	4.1	N	Reverse
4557	EMILIA_2ND_MAINSHOCK	20120529	MIR03	6.0	9.8	N	Reverse

Fig. 16. Consistency plots of spectral compatibility sets discussed in previous Fig. 15. The left column shows the compatible sets associated with the best consistency performance, while the right column shows compatible sets corresponding to lower consistency performance.

compatibility. This suggested a reduction of the IF threshold to 2.0, so in the second preselection round a new series of 35 candidate signals was obtained. The signals in this series were equalized from natural ones, recorded during the mainshock of the Central Italy sequence at AMT station. Using the input criteria resulting from the consistency analysis, the multiparametric median values have confidence levels of 86th percentile for PGA, 83rd percentile for average PSA, 56th percentile (60th for Normal Fault and 50th for Reverse Fault) for Normalized Arias Index (eq. 2), and finally, 54th percentile (35th for Normal Fault and 56th for Reverse Fault) for the spectral shape representativeness (PGA on average PSA ratio). The role of the consistency analysis can be highlighted by noting that, when using the default value of ΔPGA (±

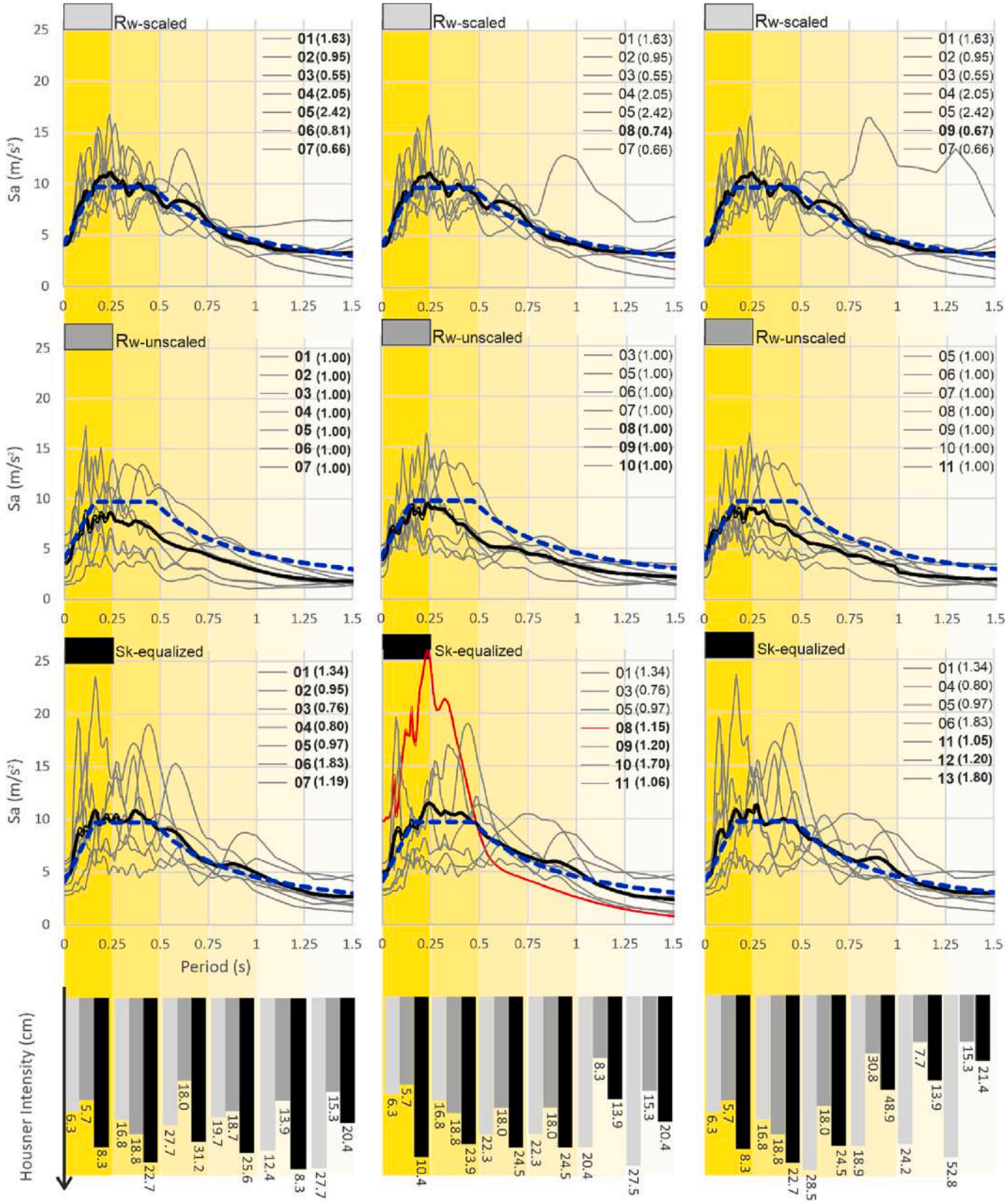

Fig. 17. Results of the comparative analysis between webRexel, scaled (Rw-scaled) and Unscaled (Rw-unscaled), and SHAKER, Sk-equalized. A progressive number of signals are reported and the signals appearing for the first time in the combined GMsets are in bold; scaling factors are in brackets. The target spectrum is blue and red is the GM coming from the natural one recorded at AMT 24th August 2016 along the EW direction. The bar plots represent the partialized Housner intensity, in centimeters, which insists on different spectral sectors (longitudinal yellow bars). Dark yellow sectors expect greater energy in the near normal fault condition. (For interpretation of the references to colour in this figure legend, the reader is referred to the web version of this article.)

20%), a smaller set (19 signals) with a very high incoherence is provided. This is mainly due to the 5th percentile (best 50th) of confidence for spectral shape representativeness related to Normal Fault sources (23rd for Reverse Fault). All other parameters decreased around the 60-70th percentile of confidence too, and the set does not contain the AMT's natural records of the mainshock.

Web-Rexel selector has been running both scaled and unscaled mode, and three sets of combinations have been performed for each compared selector system (Fig. 17). Good matchings were shown by scaled Rexel and equalized SHAKER combinations, while relevant underfit is shown by unscaled Rexel combinations. This confirms that the use of an unscaled signal selector is not sufficient to match every target spectral shape, even more, when design spectra from RSL are given. SHAKER provides a notable assortment of solutions, with half of the signals being renovated in each round. Instead, unscaled Rexel introduces only one signal, starting already from the third round. The substitution of signals in scaled Rexel introduces outlier ground motions with larger energy at longer spectral periods. In this regard, the response spectra are largely and completely exceeded by those in unscaled Rexel sets; this also occurs with scaled ones, but with minor spread. These input ground motions do not provide any contribution to the dynamic assessments and verifications. Instead, the energy equalization of SHAKER excludes such occurrences through its internal logic; all spectra cross the target and all signals cross each other. Finally, the maximum distribution of the energy shows that a greater content at periods lesser than 0.5 s happens for the set by SHAKER. In this spectral interval, the proposed system selects equalized ground motions with maximum Housner intensity values over the unscaled and scaled Rexel system by about 50%; this is also suggested by consistency analysis. In this way, the natural event – specifically, the AMT record detected along the EW direction (the bigger one) – can appear in one of the GMsets (the second) provided by SHAKER. Here, the ground motion equalized with >15% scaling suggests that the energy level of the natural event recorded at AMT meets the expected hazard, as well as the SHAKER system consistency. The latter, unlike Web Rexel, included this event in the spectral compatible sets.

6. Conclusions

Based on a different approach compared to the traditional selector systems, a new natural ground motion set selector to satisfy hazard spectral compatibility was proposed. The selection is controlled by non-mutually-exclusive multiparametric criteria, with reference to the Magnitude distance pairs and minimum and maximum thresholds for PGA and scaling factors. This system outputs ground motion sets containing signals with the same spectral energy level as the target hazard spectrum. The resulting set has a large spectral assortment, without predominant/subordinated ground motion presences, and all sectors of the spectral interval have a confrontable energy content. The core of the system is the consistency analysis, which allows moving from a common mathematical expedient of matching to a stochastic consistency model. Its solutions are supported by confidence levels and include the historical local hazard in the regional database. The characteristic parameters subjected to this confidence analysis are: the spectral energy, by PGA and average PSA, and a new parameter, Normalized Aria Intensity (IA-PGA) introduced to quantify the relative duration of the ground motions. Compounding these, the spectral shape parameter given by PGA to average-PSA ratio.

The parametric correlation analysis on the whole database highlights a notable correlation between Magnitude and distance couples and the ground motion consistency parameters. Spectral energy concentration and migration, joined with ground motion time length, cannot be taken into account by simple scaling, but must involve also all the other signals – including the unscaled ones - that fulfill the selection criteria. Moreover, the correlation trends split also in relation to the focal mechanism of sources. Sensitivity analysis, performed on three sites characterized by different seismic hazard levels, shows the importance of consistency analysis to support the selection criteria, as well as the inadequacy of the design of uniform spectra in meeting the spectral consistency shape. Then, comparative analysis highlights the higher efficacy of the proposed system in selecting waveforms that are close to real ones, compared to traditional systems.

Finally, the proposed system introduces a new concept of selection based on the confidence and verisimilitude of waveforms, subjected to a strict control of spectral energy level distributions. This last parameter may be a new way to define the local hazard and concerning that, the future advancements of the proposed model will be aimed at defining consistent design spectra and the related compatible ground motion sets.

Acknowledgments and author contributions

Thanks to ReLuis (Consortium of the Network of Seismic and Structural Engineering of the University Laboratories) for funding the open access publication through the grant for guidelines experimentation on risk classification and management, safety assessment, and monitoring of existing bridges (DM 204, 1 July 2022) - Prof. Giuseppe Sappa's Research Group. A special thanks to Prof. Nicola Nisticò for introducing us to the engineering issues regarding the correct selection of input ground motions in non-linear dynamic analysis.

Gerardo Grelle is the method idealizer and code developer, Claudia Madiai supportersupported the validation and Giuseppe Sappa is the project coordinator.

Declaration of Competing Interest

The authors declare that they have no known competing financial interests or personal relationships that could have appeared to influence the work reported in this paper.

Data availability

Data will be made available on request.

References

Akkar, S., Sandıkkaya, M.A., Bommer, J.J., 2014. Empirical ground-motion models for point- and extended-source crustal earthquake scenarios in Europe and the Middle East. Bull. Earthq. Eng. https://doi.org/10.1007/s10518-013-9461-4.

Alatik, L., Abrahamson, N., 2010. An improved method for nonstationary spectral matching. Earthquake Spectra. https://doi.org/10.1193/1.3459159.

Ambraseys, N.N., 1995. The prediction of earthquake peak ground acceleration in europe. Earthq. Eng. Struct. Dyn. 24. https://doi.org/10.1002/eqe.4290240402.

Ambraseys, N.N., Simpson, K.A., Bommer, J.J., 1996. Prediction of horizontal response spectra in Europe. Earthq. Eng. Struct. Dyn. 25. https://doi.org/10.1002/(SICI)1096-9845(199604)25.

Amini, D., Maghoul, P., Perret, D., Gatmiri, B., 2022. Two-dimensional basin-scale seismic site effects in the Kitimat Valley, British Columbia, Canada: a practical example of using a fast hybrid FE/BE method. Eng. Geol. 311, 106872 https://doi.org/10.1016/j.enggeo.2022.106872.

Angell, M.M., Geophysics, A.O.A., Hanson, K., Youngs, R., Abramson, H., 2003. Probabilistic fault displacement hazard assessment for flowlines and export pipelines, mad dog and atlantis field developments, Deepwater Gulf of Mexico. In: Proceedings of the Annual Offshore Technology Conference. https://doi.org/10.4043/15402-ms.

Baker, J.W., Lee, C., 2018. An improved algorithm for selecting ground motions to match a conditional spectrum. J. Earthq. Eng. https://doi.org/10.1080/13632469.2016.1264334.

Barani, S., Spallarossa, D., Bazzurro, P., 2009. Disaggregation of probabilistic ground-motion Hazard in Italy. Bull. Seismol. Soc. Am. https://doi.org/10.1785/0120080348.

Beyer, K., Bommer, J.J., 2007. Selection and scaling of real accelerograms for bi-directional loading: a review of current practice and code provisions. J. Earthq. Eng. https://doi.org/10.1080/13632460701280013.

Bhanu, V., Chandramohan, R., Sullivan, T.J., 2021. Influence of ground motion duration on the dynamic deformation capacity of reinforced concrete frame structures. Earthquake Spectra 37. https://doi.org/10.1177/87552930211033879.

Blázquez, R., López-Querol, S., 2006. Generalized densification law for dry sand subjected to dynamic loading. Soil Dyn. Earthq. Eng. https://doi.org/10.1016/j.soildyn.2005.09.001.

Bommer, J.J., Acevedo, A.B., 2004. The use of real earthquake accelerograms as input to dynamic analysis. J. Earthq. Eng. 8 https://doi.org/10.1080/13632460409350521.

Bommer, J.J., Crowley, H., 2006. The influence of ground-motion variability in earthquake loss modelling. Bull. Earthq. Eng. https://doi.org/10.1007/s10518-006-9008-z.
Bommer, J.J., Scott, S.G., Sarma, S.K., 2000. Hazard-consistent earthquake scenarios. Soil Dyn. Earthq. Eng. https://doi.org/10.1016/S0267-7261(00)00012-9.
Bommer, J.J., Magenes, G., Hancock, J., Penazzo, P., 2004. The influence of strong-motion duration on the seismic response of masonry structures. Bull. Earthq. Eng. https://doi.org/10.1023/B:BEEE.0000038948.95616.bf.
Castro, G., Enos, J.L., France, J.W., Poulos, S.J., 1983. Liquefaction Induced by Cyclic Loading.
Cattari, S., Camilletti, D., Lagomarsino, S., Bracchi, S., Rota, M., Penna, A., 2018. Masonry Italian Code-Conforming buildings. Part 2: Nonlinear Modelling and Time-history Analysis. J. Earthq. Eng. 22 https://doi.org/10.1080/13632469.2018.1541030.
Chandramohan, R., Baker, J.W., Deierlein, G.G., 2014. Hazard-consistent ground motion duration: Calculation procedure and impact on structural collapse risk. In: NCEE 2014 - 10th U.S. National Conference on Earthquake Engineering: Frontiers of Earthquake Engineering. https://doi.org/10.4231/D30G3GZ7T.
Chang, S.J., Jeong, Y.S., Eem, S.H., Choi, I.K., Park, D.U., 2021. Evaluation of MCC seismic response according to the frequency contents through the shake table test. Nucl. Eng. Technol. 53, 1345–1356. https://doi.org/10.1016/J.NET.2020.10.002.
Corigliano, M., Lai, C.G., Rota, M., Strobbia, C.L., 2012. ASCONA: Automated selection of compatible natural accelerograms. Earthquake Spectra. https://doi.org/10.1193/1.4000072.
Cornell, C.A., 1969. Probability-based structural code. Am Concrete Inst-J 66 (12), 974–985.
D'Amico, S., Akinci, A., Pischiutta, M., 2018. High-frequency ground-motion parameters from weak-motion data in the Sicily Channel and surrounding regions. Geophys. J. Int. 214 https://doi.org/10.1093/gji/ggy107.
Decanini, L.D., Mollaioli, F., 2001. An energy-based methodology for the assessment of seismic demand. Soil Dyn. Earthq. Eng. https://doi.org/10.1016/S0267-7261(00)00102-0.
Du, P., Kibbe, W.A., Lin, S.M., 2006. Improved peak detection in mass spectrum by incorporating continuous wavelet transform-based pattern matching. Bioinformatics. https://doi.org/10.1093/bioinformatics/btl355.
Du, W., Yu, X., Ning, C.L., 2020. Influence of earthquake duration on structural collapse assessment using hazard-consistent ground motions for shallow crustal earthquakes. Bull. Earthq. Eng. 18 https://doi.org/10.1007/s10518-020-00814-2.
Du, W., Long, S., Ning, C.L., 2022. An Algorithm for Selecting Spatially Correlated Ground Motions at Multiple Sites under Scenario Earthquakes. J. Earthq. Eng. 26 https://doi.org/10.1080/13632469.2019.1688736.
Ergun, M., Ates, S., 2014. Comparing of the effects of scaled and real earthquake records on structural response. Earthquake Struct. https://doi.org/10.12989/eas.2014.6.4.375.
Falcone, G., Mendicelli, A., Mori, F., Fabozzi, S., Moscatelli, M., Occhipinti, G., Peronace, E., 2020. A simplified analysis of the total seismic hazard in Italy. Eng. Geol. 267 https://doi.org/10.1016/j.enggeo.2020.105511.
Forte, G., Chioccarelli, E., De Falco, M., Cito, P., Santo, A., Iervolino, I., 2019. Seismic soil classification of Italy based on surface geology and shear-wave velocity measurements. Soil Dyn. Earthq. Eng. 122 https://doi.org/10.1016/j.soildyn.2019.04.002.
Galadini, F., Falcucci, E., Galli, P., Giaccio, B., Gori, S., Messina, P., Moro, M., Saroli, M., Scardia, G., Sposato, A., 2012. Time intervals to assess active and capable faults for engineering practices in Italy. Eng. Geol. https://doi.org/10.1016/j.enggeo.2012.03.012.
Gao, Y., Wu, Y., Li, D., Zhang, N., Zhang, F., 2014. An improved method for the generating of spectrum compatible time series using wavelets. Earthquake Spectra. https://doi.org/10.1193/051912EQS190M.
Goulet, C.A., Haselton, C.B., Mitrani-Reiser, J., Beck, J.L., Deierlein, G.G., Porter, K.A., Stewart, J.P., 2007. Evaluation of the seismic performance of a code-conforming reinforced-concrete frame building - from seismic hazard to collapse safety and economic losses. Earthq. Eng. Struct. Dyn. https://doi.org/10.1002/eqe.694.
Grelle, G., Guadagno, F.M., 2013. Regression analysis for seismic slope instability based on a double phase viscoplastic sliding model of the rigid block. Landslides 10, 583–597. https://doi.org/10.1007/s10346-012-0350-8.
Grelle, G., Revellino, P., Guadagno, F.M., 2011. Methodology for seismic and post-seismic stability assessment of natural clay slopes based on a viscoplastic behaviour model in simplified dynamic analysis. Soil Dyn. Earthq. Eng. 31, 1248–1260. https://doi.org/10.1016/j.soildyn.2011.05.005.
Grelle, G., Bonito, L., Lampasi, A., Revellino, P., Guerriero, L., Sappa, G., Guadagno, F. M., 2016. SiSeRHMap v1.0: a simulator for mapped seismic response using a hybrid model. Geosci. Model Dev. 9, 1567–1596. https://doi.org/10.5194/gmd-9-1567-2016.
Grelle, G., Gargini, E., Facciorusso, J., Maresca, R., Madiai, C., 2020. Seismic site effects in the Red Zone of Amatrice hill detected via the mutual sustainment of experimental and computational approaches. Bull. Earthq. Eng. 18, 1955–1984. https://doi.org/10.1007/s10518-019-00777-z.
Grelle, G., Bonito, L., Rosalba, M., Iacurto, S., Madiai, C., Revellino, P., Sappa, G., 2021. Topographic effects observed at Amatrice hill during the 2016–2017 Central Italy seismic sequence. Earthq. Eng. Eng. Vib. 20 https://doi.org/10.1007/s11803-021-2005-z.
Hancock, J., Watson-Lamprey, J., Abrahamson, N.A., Bommer, J.J., Markatis, A., McCoy, E.M.M.A., Mendis, R., 2006. An improved method of matching response spectra of recorded earthquake ground motion using wavelets. J. Earthq. Eng. https://doi.org/10.1080/13632460609350629.
Hildyard, M., Napier, J.A.L., Spottiswoode, S.M., Sellers, E., Linzer, L.M., Kataka, M., 2009. New criteria for rockmass stability and control using integration of seismicity and numerical modelling. In: SIMRAC Report.
Iervolino, I., Cornell, C.A., 2005. Record selection for nonlinear seismic analysis of structures. Earthquake Spectra. https://doi.org/10.1193/1.1990199.
Iervolino, I., Galasso, C., Cosenza, E., 2010. REXEL: Computer aided record selection for code-based seismic structural analysis. Bull. Earthq. Eng. https://doi.org/10.1007/s10518-009-9146-1.
Iervolino, I., Spillatura, A., Bazzurro, P., 2018. Seismic Reliability of Code-Conforming Italian Buildings. J. Earthq. Eng. 22 (2), 5–27. https://doi.org/10.1080/13632469.2018.1540372.
International Code Council (ICC), 2018. 2018 International Building Code Illustrated Handbook. International Code Council.
Jibson, R.W., Tanyaş, H., 2020. The influence of frequency and duration of seismic ground motion on the size of triggered landslides—a regional view. Eng. Geol. 273, 105671 https://doi.org/10.1016/J.ENGGEO.2020.105671.
Katsanos, E.I., Sextos, A.G., Manolis, G.D., 2010. Selection of earthquake ground motion records: a state-of-the-art review from a structural engineering perspective. Soil Dyn. Earthq. Eng. https://doi.org/10.1016/j.soildyn.2009.10.005.
Kottke, A., Rathje, E.M., 2008. A semi-automated procedure for selecting and scaling recorded earthquake motions for dynamic analysis. Earthquake Spectra. https://doi.org/10.1193/1.2985772.
Lanzo, G., Pagliaroli, A., Scasserra, G., 2015. Selection of ground motion time histories for the nonlinear analysis of earth dams. In: Geotechnical Engineering for Infrastructure and Development - Proceedings of the XVI European Conference on Soil Mechanics and Geotechnical Engineering. ECSMGE, p. 2015.
Lasley, S.J., Green, R.A., Rodriguez-Marek, A., 2017. Number of equivalent stress cycles for liquefaction evaluations in active tectonic and stable continental regimes. J. Geotech. Geoenviron. https://doi.org/10.1061/(ASCE)GT.1943-5606.0001629.
Laurendeau, A., Cotton, F., Ktenidou, O.J., Bonilla, L.F., Hollender, F., 2013. Rock and stiff-soil site amplification: Dependency on VS30 and Kappa (κ0). Bull. Seismol. Soc. Am. 103, 3131–3148. https://doi.org/10.1785/0120130020.
Liu, A.H., Stewart, J.P., Abrahamson, N.A., Moriwaki, Y., 2001. Equivalent Number of Uniform stress Cycles for Soil Liquefaction Analysis. J. Geotech. Geoenviron. https://doi.org/10.1061/(asce)1090-0241(2001)127:12(1017).
Lombardi, L., de Luca, F., 2018. Linear Time-History Analysis as EC8-compliant design method: What seismic input selection?. In: 11th National Conference on Earthquake Engineering 2018, NCEE2018: Integrating Science, Engineering, and Policy.
Luzi, L., Puglia, R., Russo, E., D'Amico, M., Felicetta, C., Pacor, F., Lanzano, G., Çeken, U., Clinton, J., Costa, G., Duni, L., Farzanegan, E., Gueguen, P., Ionescu, C., Kalogeras, I., Özener, H., Pesaresi, D., Sleeman, R., Strollo, A., Zare, M., 2016. The engineering strong-motion database: a platform to access pan-European accelerometric data. Seismol. Res. Lett. 87 https://doi.org/10.1785/0220150278.
Manfredi, V., Masi, A., Güney Özcebe, A., Paolucci, R., Smerzini, C., 2022. Selection and spectral matching of recorded ground motions for seismic fragility analyses. Bull. Earthq. Eng. https://doi.org/10.1007/s10518-022-01393-0.
Meletti, C., Visini, F., D'Amico, V., Rovida, A., 2016. Seismic hazard in Central Italy and the 2016 amatrice earthquake. Ann. Geophys. https://doi.org/10.4401/AG-7248.
Monti, G., Nisticò, N., 2002. Simple Probability-based Assessment of Bridges under Scenario Earthquakes. J. Bridg. Eng. https://doi.org/10.1061/(asce)1084-0702(2002)7:2(104).
Nakamura, S., Wakai, A., Umemura, J., Sugimoto, H., Takeshi, T., 2014. Earthquake-induced landslides: distribution, motion and mechanisms. Soils Found. https://doi.org/10.1016/j.sandf.2014.06.001.
Nettles, M., Ekström, G., 2004. Long-period source characteristics of the 1975 Kalapana, Hawaii, earthquake. Bull. Seismol. Soc. Am. https://doi.org/10.1785/0120030090.
Newmark, N., Hall, W., 1982. Earthquake Spectra and Design. EERI Monographs.
Nong, Z., Park, S.S., Jeong, S.W., Lee, D.E., 2020. Effect of cyclic loading frequency on liquefaction prediction of sand. Appl. Sci.(Switzerland) 10. https://doi.org/10.3390/app10134502.
Panza, G.F., Bela, J., 2020. NDSHA: a new paradigm for reliable seismic hazard assessment. Eng. Geol. 275 https://doi.org/10.1016/j.enggeo.2019.105403.
Paolucci, R., Pacor, F., Puglia, R., Ameri, G., Cauzzi, C., Massa, M., 2011. Record processing in ITACA, the New Italian strong-motion database. Geotechn. Geol. Earthquake Eng. https://doi.org/10.1007/978-94-007-0152-6_8.
Rathje, E.M., Saygili, G., 2009. Probabilistic assessment of earthquake-induced sliding displacements of natural slopes. Bull. N. Z. Soc. Earthq. Eng. https://doi.org/10.5459/bnzsee.42.1.18-27.
Sabetta, F., Pugliese, A., 1996. Estimation of response spectra and simulation of nonstationary earthquake ground motions. Bull. Seismol. Soc. Am. 86, 337–352.
Sgobba, S., Puglia, R., Pacor, F., Luzi, L., Russo, E., Felicetta, C., Lanzano, G., D'amico, M., Baraschino, R., Baltzopoulos, G., Iervolino, I., 2019. Rexelweb: A Tool for Selection of Ground-Motion Records from the Engineering Strong Motion Database (Esm), in: Earthquake Geotechnical Engineering for Protection and Development of Environment and Constructions- Proceedings of the 7th International Conference on Earthquake Geotechnical Engineering, 2019.
Shiwua, A.J., Rutman, Y., 2016. Assessment of seismic input energy by means of new definition and the application to earthquake resistant design. Archit. Eng. https://doi.org/10.23968/2500-0055-2016-1-4-26-35.
Stafford, P.J., Bommer, J.J., 2009. Theoretical consistency of common record selection strategies in performance-based earthquake engineering. Geotech. Geol. Earthquake Eng. 13, 49–58.
Sun, X.Y., Han, J.P., Dang, Y., Zhou, Y., 2018. Effect of ground motion duration on seismic fragility of RC frames with different beam-column joint failure modes. Gongcheng Lixue/Eng. Mech. 35 https://doi.org/10.6052/j.issn.1000-4750.2017.01.0089.

Tao, D., Lin, J., Lu, Z., 2019. Time-frequency energy distribution of ground motion and its effect on the dynamic response of nonlinear structures. Sustainability (Switzerland) 11. https://doi.org/10.3390/su11030702.

Thøgersen, K., Andersen Sveinsson, H., Scheibert, J., Renard, F., Malthe-Sørenssen, A., 2019. The Moment Duration Scaling Relation for Slow Rupture Arises from Transient Rupture Speeds. Geophys. Res. Lett. https://doi.org/10.1029/2019GL084436.

Tsompanakis, Y., 2014. Encyclopedia of Earthquake Engineering, Encyclopedia of Earthquake Engineering. https://doi.org/10.1007/978-3-642-36197-5.

Wang, G., Zhang, S., Zhou, C., Lu, W., 2015. Correlation between strong motion durations and damage measures of concrete gravity dams. Soil Dyn. Earthq. Eng. https://doi.org/10.1016/j.soildyn.2014.11.001.

Weatherill, G., Cotton, F., 2020. A ground motion logic tree for seismic hazard analysis in the stable cratonic region of Europe: regionalisation, model selection and development of a scaled backbone approach. Bull. Earthq. Eng. 18, 6119–6148. https://doi.org/10.1007/s10518-020-00940-x.

Woessner, J., Laurentiu, D., Giardini, D., Crowley, H., Cotton, F., Grünthal, G., Valensise, G., Arvidsson, R., Basili, R., Demircioglu, M.B., Hiemer, S., Meletti, C., Musson, R.W., Rovida, A.N., Sesetyan, K., Stucchi, M., Anastasiadis, A., Akkar, S., Engin Bal, I., Barba, S., Bard, P.Y., Beauval, C., Bolliger, M., Bosse, C., Bonjour, C., Bungum, H., Carafa, M., Cameelbeeck, T., Carvalho, A., Campos-Costa, A., Coelho, E., Colombi, M., D'amico, V., Devoti, R., Drouet, S., Douglas, J., Edwards, B., Erdik, M., Fäh, D., Fonseca, J., Fotopoulou, S., Glavatovic, B., Gómez Capera, A.A., Hauser, J., Husson, F., Kastelic, V., Kästli, P., Karatzetzou, A., Kaviris, G., Keller, N., Kierulf, H.P., Kouskouna, V., Krishnamurty, R., Lang, D., Lemoine, A., Lindholm, C., Makropoulos, K., Manakou, M., Marmureanu, G., Martinelli, F., Garcia Mayordomo, J., Mihaljevic, J., Monelli, D., Garcia-Moreno, D., Nemser, E., Pagani, M., Pinho, R., Pisani, A.R., Pitilakis, D., Pitilakis, K., Poggi, V., Radulian, M., Riga, E., Sandikkaya, M.A., Segou, M., Siegert, R., Silva, V., Stromeyer, D., Sousa, L., Sørensen, M.B., Tellez-Arenas, A., Vanneste, K., Wahlström, R., Weatherill, G., Viganò, D., Vilanova, S., Yenier, E., Zulfikar, C., Adams, J., Bommer, J.J., Bonilla, F., Faccioli, E., Gülen, L., Koller, M., Pinto, A., Pinto, P., Papaioannou, C., Peruzza, L., Scherbaum, F., Scotti, O., Stirling, M., Theodoulidis, N., Wenk, T., Zschau, J., 2015. The 2013 European Seismic Hazard Model: key components and results. Bull. Earthq. Eng. https://doi.org/10.1007/s10518-015-9795-1.

Wood, R.L., Hutchinson, T.C., 2012. Effects of ground motion scaling on nonlinear higher mode building response. Earthquake Struct. 3, 869–887. https://doi.org/10.12989/eas.2012.3.6.869.

Xu, Q., Chai, S., Zhou, S., Bao, L., Li, Q., 2022. Time-frequency characteristics of ground motion and seismic response analysis of typical structures in the Yangbi Earthquake in Yunnan Province. Adv. Civil Eng. 2022, 9998019. https://doi.org/10.1155/2022/9998019.

Zhang, S., Wang, G., Pang, B., Du, C., 2013. The effects of strong motion duration on the dynamic response and accumulated damage of concrete gravity dams. Soil Dyn. Earthq. Eng. https://doi.org/10.1016/j.soildyn.2012.11.011.